

UniCL: A Universal Contrastive Learning Framework for Large Time Series Models

Jiawei Li
HKUST (GZ)
Guangzhou, China
jli226@connect.hkust-gz.edu.cn

Haoyang Li
HKUST
Hong Kong SAR, China
hlicg@connect.ust.hk

Jingshu Peng
HKUST
Hong Kong SAR, China
jpengab@cse.ust.hk

Lei Chen
HKUST (GZ) & HKUST
Hong Kong SAR, China
leichen@cse.ust.hk

ABSTRACT

Time-series analysis plays a pivotal role across a range of critical applications, from finance to healthcare, which involves various tasks, such as forecasting and classification. To handle the inherent complexities of time-series data, such as high dimensionality and noise, traditional supervised learning methods first annotate extensive labels for time-series data in each task, which is very costly and impractical in real-world applications. In contrast, pre-trained foundation models offer a promising alternative by leveraging unlabeled data to capture general time series patterns, which can then be fine-tuned for specific tasks. However, existing approaches to pre-training such models typically suffer from *high-bias* and *low-generality* issues due to the use of predefined and rigid augmentation operations and domain-specific data training. To overcome these limitations, this paper introduces UniCL, a universal and scalable contrastive learning framework designed for pretraining time-series foundation models across cross-domain datasets. Specifically, we propose a unified and trainable time-series augmentation operation to generate pattern-preserved, diverse, and low-bias time-series data by leveraging spectral information. Besides, we introduce a scalable augmentation algorithm capable of handling datasets with varying lengths, facilitating cross-domain pretraining. Extensive experiments on two benchmark datasets across eleven domains validate the effectiveness of UniCL, demonstrating its high generalization on time-series analysis across various fields.

KEYWORDS

Foundation Model, Time Series, Data Management

1 INTRODUCTION

Time series data, which consists of sequences of real values recorded over time intervals, are prevalent in numerous real-world applications [64], including finance, healthcare, environmental monitoring, and manufacturing. Time series analysis involves various tasks such as forecasting [57] and classification [21], which are crucial for decision-making processes. However, analyzing time series data remains challenging due to their inherent properties, such as high dimensionality, noise, non-stationarity, periodicity, etc. [62]. These features pose difficulties in effectively capturing and leveraging the underlying patterns in time series data, thus impacting its practical

applications [40], highlighting the ongoing challenge of analyzing time series data across various tasks.

In general, existing time-series analysis in deep learning can be categorized into two types, supervised learning (SL)-based approaches [55, 65] and pretrained foundation model (PFM)-based approaches [23, 76]. First, SL-based approaches [26, 35, 69, 82] propose to train a deep learning model, such as transformers [43, 69, 83] and CNNs [80], on labeled time series data. However, these SL-based approaches rely on a large number of annotated time series data [24], which is often impractical in many real-world scenarios where obtaining labeled time-series data is costly or infeasible. Second, current researchers [3, 12, 36, 72] propose to first pre-train a foundation model (e.g., large language models) on time-series data, such as those initially large language models (e.g., ChatGPT [45]) developed for processing natural language. The basic idea is to first pre-train the foundation model to capture the general intrinsic patterns of time-series data. Subsequently, the foundation model can be fine-tuned on specific time-series tasks using a smaller set of labeled data. These PFM-based approaches can leverage the learned general patterns to enhance performance across a variety of tasks.

Depending on the technique employed to pre-train the foundation model, existing research [12, 28, 74] first propose to use mask-based approaches to pre-train the foundation model in time series data. They directly use the foundation model to predict the next values in a time series [3, 36, 53] or reconstruct randomly masked values of the data [12], *i.e.*, predictive objectives. However, these mask-based pre-training approaches require numerous unlabeled time-series data to enable the foundation model to capture general time-series patterns [65]. Unlike corpus data, the time-series are scarce in the open-world website [1, 37]. Consequently, these mask-based approaches achieve suboptimal performance on the downstream tasks. Recently, to alleviate the heavy reliance on numerous time series data, contrastive learning approaches [13, 39, 41, 66, 71] are proposed to augment time-series data and pre-train the foundation model based on augmented data. The basic idea is to first generate positive views for each time series data to preserve its key patterns. Then, the foundation model is optimized by maximizing the representation similarity between positive view pairs and minimizing the representation similarity between positive views and other randomly selected time series data (*i.e.*, negative views), known as contrastive objectives. This enables the pre-trained model

to distinguish patterns across different time-series data, thereby facilitating downstream tasks [40].

Nevertheless, existing CL-based pretrained foundation models suffer from two issues, i.e., *high-bias* and *low-generality* issues. First, these models typically predefine and apply a set of time series augmentation operations, such as permutation [41, 47], random masking [63, 72], and warping [14] to generate positive views. However, existing predefined operations ignore the time-series intrinsic properties, such as periodicity [48], thereby introducing high bias and noise. For instance, permutation shuffles the sequential information in time series data, potentially resulting in the loss of its inherent patterns. Consequently, the foundation models, optimized by maximizing the similarity between the generated positive views, may not capture the patterns of real time-series data, thus degrading the performance of downstream tasks [13, 72, 81]. Secondly, these models are generally pretrained within a single specific domain [39, 66, 72], such as medicine [63]. However, time series data can vary significantly across different domains (e.g., medical, traffic, and weather) in aspects of the number of variables, sequence length, and frequency (e.g., daily, weekly, monthly). Due to these variations, foundation models trained on one domain often fail to perform effectively across other domains [40]. In other words, existing approaches [63, 66, 72] need to pre-train a single foundation model for each specific domain, which is time-consuming and very costly.

To address the *high-bias* and *low-generality* issues, we propose a universal pre-trained foundation model for time series analysis. Firstly, to address the *high-bias* issue, we propose to use effective pattern-preserved augmentation operations to generate positive views for the time series data. By optimizing the foundation model on these augmented views, it becomes capable of learning and retaining the intrinsic patterns present in real-world time series data, thereby reducing bias. Secondly, to overcome *low-generality* issue, we propose to pre-train the foundation model across a diverse array of time series data from various domains. In such a way, this foundation model can learn a wide range of time series patterns specific to different domains. As a result, the foundation model can generalize on various domains and thereby facilitate their downstream tasks. However, there are three technique challenges to achieving this unified foundation model.

- There is no theoretical analysis and established metrics for preserving the patterns of time-series data with deep learning. Without these metrics, we cannot design effective augmentation operations to generate positive views that keep the intrinsic patterns.
- Due to the high variations (e.g., variable number and sequence length) in time-series data from different domains, it is challenging to design a scalable and unified augmentation algorithm that is applicable across these diverse settings.
- Last but not least, existing studies train the LLM-based encoder for time-series analysis by optimizing the predictive objective, yet, the exploration of the contrastive objective has received comparatively less attention.

To address the above technique challenges, we propose UniCL, a universal contrastive learning framework designed for pre-training time-series foundation models across diverse domains. Firstly, we empirically reveal a positive correlation between the bias of time

Table 1: Summary of important notations

Notation	Description
t, T	General time index
n	The number of variables
$\mathbf{x} \in \mathbb{R}^T$	The observed sequences of variable
$x_i \in \mathbb{R}$	The i -th value of \mathbf{x}
$\mathbf{X}^{(j)} \in \mathbb{R}^{n \times T}$	The j -th observed time series data
$\mathbf{x}^{(j,i)}$	The i -th variable in $\mathbf{X}^{(j)}$
$\mathbf{X}_{t:t+H}$	Values of \mathbf{X} between time t and $t + H$
f_θ	The encoder model for time series data
f_{θ^\dagger}	Optimized foundation model on time-series data
q_ϕ	The decoder model for prediction

series embeddings and the spectral distance between augmented and raw series. Building on this insight, we propose a unified and trainable time series augmentation operation with theoretical guarantees. Through optimization of two novel losses, our proposed operation generates spectrum-preserved, diverse, and low bias augmented series. Secondly, to tackle high variations in datasets and enable large-scale automatic pre-training, we propose a scalable and unified augmentation algorithm. This algorithm utilizes spectrum-preserved time-series segmentation, augmenting each subseries individually. We demonstrate that the difference in convergence loss between the scalable and non-scalable algorithms can be bounded. Thirdly, to fully leverage the potential of the LLM backbone, we train a transformer-based encoder on 40 cross-domain datasets, initialized with pre-trained weights from the text encoder of CLIP [49], owing to our shared contrastive objectives. We summarize the novel contributions of this paper as follows.

- We present UniCL, an end-to-end general framework for pre-training large foundation time-series models based on contrastive learning, capable of handling high variation time-series datasets.
- We reveal the factor of representation bias based on a novel metric, and propose a unified and trainable augmentation operation with theoretical guarantees. We then propose two novel losses to facilitate the optimization of this operation.
- We propose a scalable and unified algorithm to handle data with varied length by pattern-preserved segmentation and concatenation, and demonstrate bounded convergence loss differences between scalable and non-scalable algorithms.
- To the best of our knowledge, we are the first to train the LLM backbone with contrastive objectives for general time-series analysis. We train the UniCL on 40 cross-domain datasets, and provide a comprehensive evaluation of its performance across two downstream tasks.

2 PRELIMINARIES AND RELATED WORKS

In this section, we first introduce the basic concepts in time-series data analysis and then introduce the foundation models for time-series data analysis. The important notations are listed in Tab. 1.

2.1 Time-series Data Analysis

Time series data are a set of sequences of observations where each sequence corresponds to a different variable, and all sequences

are recorded over the same time periods. Time series data plays a crucial role in various fields [64], such as economics, finance, environmental science, and engineering. Formally, a time series data instance with n variables over time T can be denoted as $\mathbf{X} = [\mathbf{x}^{(i)}]_{i=1}^n \in \mathbb{R}^{n \times T}$, where $\mathbf{x}^{(i)} = [x_1^{(i)}, x_2^{(i)}, \dots, x_T^{(i)}] \in \mathbb{R}^T$ in the observed real value of variable $x^{(i)}$ from time 1 to T . In general, if the number of variable n is 1 (resp. $n \geq 2$), this time-series data is called univariate (resp. multivariate) time-series data. Time-series analysis involves various tasks such as forecasting [30] and classification [21]. We first give a general time-series data analysis problem definition for various tasks. Formally, given a training time-series data $D_{task} = \{\mathbf{X}^{(j)}, \mathbf{Y}^{(j)}\}_{j=1}^m$ with m instances for a task, where $\mathbf{X}^{(j)} = [\mathbf{x}^{(j,i)}]_{i=1}^n$ denotes each time series instance and $\mathbf{Y}^{(j)}$ is the label of $\mathbf{X}^{(j)}$, the target is to supervised train an encoder model f_θ and a simple decoder model q_ϕ (e.g., simple linear regression model [72]) on data D_{task} . The encoder model f_θ is used to encode each time-series data $\mathbf{X}^{(j)}$ to an embedding matrix with D dimensions $\mathbf{Z}^{(j)} = f_\theta(\mathbf{X}^{(j)}) \in \mathbb{R}^{n \times D}$. Then the decoder model q_ϕ will use the $\mathbf{Z}^{(j)}$ to predict the task labels $\hat{\mathbf{Y}}^{(j)} = q_\phi(\mathbf{Z}^{(j)})$. In general, the parameters of the encoder model f_θ and the decoder model q_ϕ can be optimized by minimizing the task loss $\mathcal{L}_{task}(\cdot)$ as follows:

$$\theta^*, \phi^* = \arg \min_{\theta, \phi} \mathcal{L}_{task}(f_\theta, q_\phi, D_{task}) = \sum_{j=1}^m l_{task}(\hat{\mathbf{Y}}^{(j)}, \mathbf{Y}^{(j)}). \quad (1)$$

Then, we discuss how to adapt this definition for each specific task as follows.

- **Time-series Classification Task.** The target is to predict the label $y^{(j)} \in \mathcal{Y}$ of each time-series data instance $\mathbf{X}^{(j)}$. In general, $D_{task} = \{\mathbf{X}^{(j)}, \mathbf{y}^{(j)}\}_{j=1}^m$, where $\mathbf{y}^{(j)} \in \{0, 1\}^{\mathcal{Y}}$ is multiple-label ground truth of $\mathbf{X}^{(j)}$. Based on cross-entropy, the classification loss $\mathcal{L}_{cl}(\cdot)$ [58, 59] can be defined as: $\mathcal{L}_{cl}(f_\theta, q_\phi, D_{task}) = \frac{1}{m} \sum_{j=1}^m \sum_{i=1}^{|\mathcal{Y}|} \mathbf{y}^{(j)}[i] \log p_{\mathbf{y}^{(j)}}[i]$, where $p_{\mathbf{y}^{(j)}}[i]$ is the predicted probability of each label $\mathbf{y}^{(j)}[i]$ for data $\mathbf{X}^{(j)}$.
- **Time-series Forecasting Task.** The target is to predict the future values $\mathbf{X}_{t:t+H_f} \in \mathbb{R}^{n \times H_f}$ of a time-series data based on the previous observation $\mathbf{X}_{t-H_p:t} \in \mathbb{R}^{n \times H_p}$, where H_p is the look back window size, and H_f denotes the number of future prediction values. In general, $D_{task} = \{\mathbf{X}_{t-H_p:t}^{(j)}, \mathbf{X}_{t:t+H_f}^{(j)}\}_{j=1}^m$, and forecasting loss $\mathcal{L}_{fl}(\cdot)$ [22, 36] can be defined as $\mathcal{L}_{fl}(f_\theta, q_\phi, D_{task}) = \frac{1}{m} \sum_{j=1}^m \|\mathbf{X}_{t:t+H_f}^{(j)} - \hat{\mathbf{X}}_{t:t+H_f}^{(j)}\|_2^2$, where $\hat{\mathbf{X}}_{t:t+H_f}^{(j)} = q_\phi(f_\theta(\mathbf{X}_{t-H_p:t}^{(j)}))$ is the predicted values by the encoder and decoder models.

To handle each specific task in time-series analysis, existing research [35, 69, 82] propose to prepare the training data set. Then, they train deep learning models, such as transformers and convolutional neural networks (CNNs), on labeled time series data. However, these approaches need substantial labeled data, which is time-consuming and very costly [31].

2.2 Foundation Models for Time-series Data

To alleviate the reliance on labeled data, current researchers propose to learn a foundation model that captures the general patterns of time-series data and then fine-tune this foundation model with limited labels for the downstream tasks.

2.2.1 Pretrained Foundation Models. In general, existing pretrained foundation models for time-series data analysis can be categories into the following three types, i.e., *pretrained language model-based*, *mask-based*, and *contrastive learning (CL)-based* foundation models.

1) Pretrained Language Models. Recently, the language models (LMs) pretrained on numerous corpus data, such as BERT [11], T5 [51], LLaMA [61], and GPT [50], have demonstrated their strong text understanding ability in natural language processing tasks, such as question answering.

These LMs employ transformer models with self-attention mechanisms to capture long-range dependencies in data, which have the potential to capture complex temporal dependencies in time-series data. Therefore, several researchers [32, 42] directly take these pretrained LMs as the foundation model f_θ^* and propose to apply these pretrained LMs in the time-series data analysis tasks. The basic idea is to propose time-series data encoding approaches to transform the time-series data into a text-like format that can be processed by language models. For instance, LLMTIME [42] encodes time-series as a string of numerical digits, with each digit separated by spaces. LSTPrompt [32] and PromptCast [70] incorporate domain information (e.g., traffic, weather) and frequency (e.g., hour, day) into template-based descriptions, embedding them using a text tokenizer to guide the LLM.

However, LMs are inherently designed for handling text data, which is discrete and categorical, whereas time-series data is usually continuous and numeric. Therefore, existing LMs cannot effectively capture the patterns and semantics of time-series data, leading to suboptimal performance on time-series tasks. To overcome this problem, current researchers propose mask-based [12, 74] and CL-based [72, 78] foundation models pretrained on time-series directly for time-series tasks.

2) Mask-based Foundation Models. Mask-based foundational models are typically pre-trained using tasks where specific values in the input time-series are masked, and the model is trained to predict them based on contextual information. Based on the prediction targets, existing approaches can be classified into reconstruction-based [12, 16, 28, 74] and prediction-based [3, 22, 37]. In reconstruction-based methods, a binary random mask $\mathbf{M} \in \{0, 1\}^{n \times T}$ is generated to mask the input series as $\mathbf{X}^{(j)} \odot \mathbf{M}^{(j)}$. Then, the pretext task is to optimize the reconstruction loss [74], which is defined as follows:

$$\mathcal{L}_{rl} = \frac{1}{m} \sum_{j=1}^m \|\mathbf{X}^{(j)} \odot (1 - \mathbf{M}^{(j)}) - \hat{\mathbf{X}}^{(j)} \odot (1 - \mathbf{M}^{(j)})\|_2^2, \quad (2)$$

where $\hat{\mathbf{X}}^{(j)}$ is the predicted value. In prediction-based methods, models are trained to predict future values directly, with a typical prediction loss [3] defined as follows:

$$\mathcal{L}_{pl} = \frac{1}{m} \sum_{j=1}^m \|\mathbf{X}_{t:t+H_f}^{(j)} - \hat{\mathbf{X}}_{t:t+H_f}^{(j)}\|_2^2. \quad (3)$$

However, masked modeling necessitates abundant data for effective representation learning due to its reliance on self-encoding reconstruction and prediction objectives [65], and masked values are often easily predicted from neighboring time points [8]. The availability of large-scale datasets are required to ensure that the model is exposed to diverse patterns and variations in the data.

Algorithm 1: The contrastive learning-based time-series foundation models on downstream tasks.

Input: $D_{train} = \{\{X^{(j)}\}_{j=1}^m\}$,
 $D_{task} = \{\{X^{(j)}\}_{j=1}^{m'}, \{Y^{(j)}\}_{j=1}^{m'}\}$, the augmentation family \mathcal{T} , the encoder f_θ , the decoder q_ϕ , epoch number T

Output: The encoder f_{θ^*} and the decoder q_{ϕ^*}
 // Contrastive learning without labels

```

1 for  $i = 1$  to  $T$  do
2   for each  $X^{(j)} \in D_{train}$  do
3     for  $i = 1$  to  $n$  do
4       draw two operation  $\tilde{t}^{(i)}, \hat{t}^{(i)} \sim \mathcal{T}$ 
5        $\tilde{x}^{(j,i)}, \hat{x}^{(j,i)} \leftarrow \tilde{t}^{(i)}(x^{(j,i)}), \hat{t}^{(i)}(x^{(j,i)})$ 
6    $\theta^* = \arg \min_{\theta} \frac{1}{2mn} \sum_{j=1}^m \sum_{i=1}^n l_{cl}(f_\theta, \tilde{x}^{(j,i)}, \hat{x}^{(j,i)}, Neg(\cdot))$ 
  // Decoder training with labels
7  $\phi^* = \arg \min_{\phi} \mathcal{L}_{task}(q_\phi, f_{\theta^*}, D_{task})$ 
8 Return the trained encoder  $f_{\theta^*}$  and the decoder  $q_{\phi^*}$ 

```

3) Contrastive Learning-based Foundation Models. Contrastive learning aims to train the encoder f_θ by contrasting between positive and negative samples, and augmentation contrast is one of the most widely used contrastive frameworks [75]. Specifically, given a family of augmentations \mathcal{T} , data augmentation operations $\tilde{t}^{(i)}, \hat{t}^{(i)} \sim \mathcal{T}$ are applied to create positive views $\tilde{X}^{(j)} = [\tilde{x}^{(j,i)}]_{i=1}^n$ and $\hat{X}^{(j)} = [\hat{x}^{(j,i)}]_{i=1}^n$, where $\tilde{x}^{(j,i)} = \tilde{t}^{(i)}(x^{(j,i)})$ and $\hat{x}^{(j,i)} = \hat{t}^{(i)}(x^{(j,i)})$. The positive pairs $(\tilde{x}^{(j,i)}, \hat{x}^{(j,i)})_{i=1}^n$ are expected to retain crucial temporal information, and the corresponding representations, $\tilde{z}^{(j,i)} = f_\theta(\tilde{x}^{(j,i)})$ and $\hat{z}^{(j,i)} = f_\theta(\hat{x}^{(j,i)})$, should exhibit proximity within the embedding space. The negative views of $\tilde{x}^{(j,i)}$, denoted as $Neg(\tilde{x}^{(j,i)})$, comprise a set of time-series that exhibit dissimilarity to $\tilde{x}^{(j,i)}$. A typical choice [72] is $Neg(\tilde{x}^{(j,i)}) = \{\{\tilde{x}^{(j,k)}\}_{k \neq i} \cup \{\hat{x}^{(j,k)}\}_{k=1}^n\}$. Similarly, $Neg(\hat{x}^{(j,i)}) = \{\{\hat{x}^{(j,k)}\}_{k \neq i} \cup \{\tilde{x}^{(j,k)}\}_{k=1}^n\}$. To promote proximal representations of positive pairs while ensuring distant representations of negative views, the encoder f_θ is optimized by the contrastive loss $l_{cl}(\cdot)$:

$$\theta^\dagger = \arg \min_{\theta} \frac{1}{2mn} \sum_{j=1}^m \sum_{i=1}^n l_{cl}(f_\theta, \tilde{x}^{(j,i)}, \hat{x}^{(j,i)}, Neg(\cdot)) \quad (4)$$

One widely used l_{cl} [6] is defined as:

$$\begin{aligned}
& l_{cl}(f_\theta, \tilde{x}^{(j,i)}, \hat{x}^{(j,i)}, Neg(\cdot)) \\
&= -\log \frac{\exp(\text{sim}(\tilde{z}^{(j,i)}, \hat{z}^{(j,i)})/\tau)}{\sum_{\mathbf{x} \in Neg(\tilde{x}^{(j,i)})} \exp(\text{sim}(\tilde{z}^{(j,i)}, f_\theta(\mathbf{x}))/\tau)} \\
& -\log \frac{\exp(\text{sim}(\hat{z}^{(j,i)}, \tilde{z}^{(j,i)})/\tau)}{\sum_{\mathbf{x} \in Neg(\hat{x}^{(j,i)})} \exp(\text{sim}(\hat{z}^{(j,i)}, f_\theta(\mathbf{x}))/\tau)}
\end{aligned} \quad (5)$$

Where τ represents the temperature parameter, and $\text{sim}(\cdot)$ denotes the similarity function.

Existing contrastive learning approaches mainly differ in positive view generation, and can be classified into two types: context-based and augmentation-based. Context-based approaches [25, 60, 72]

generally advocate contextual consistency, considering sub-series with close temporal relationships as positive views. For example, TS2Vec [72] randomly selects two overlapping time segments as positive pairs. Other researchers [25, 60] opt for temporal neighborhood sub-series as positive pairs. However, akin to masked modeling, context-based methods are reliant on observed data and may perform poorly on unseen data, thereby failing to address the issue of data-scarcity. Instead, augmentation-based methods can generate diverse time-series based on observed data, improving the generality of the model. Current augmentation-based methods utilize pre-defined data augmentation operation, such as jittering [13, 52, 71], scaling [66], permutation [41, 47], magnitude warping [14], masking [63, 72], and pooling [29]. Some researchers [33, 78] also apply perturbation in the frequency domain. To further improve the generality of the model, CLUDA [46] adopts a composition of operations to generate positive views. However, relying on pre-defined operations entails a dependence on expert knowledge [40] and is susceptible to inductive bias [56]. Some researchers [13, 72] have observed that data augmentation is data-dependent, and inappropriate augmentations can lead to poorly learned representations. A more recent study [39] employs meta-learning to select augmentation operations adaptively based on criteria of fidelity and variety. Nonetheless, they still rely on a pre-defined set of augmentations.

2.2.2 Fine-tuning Time-series Foundation Model on Downstream Tasks. Then, the time-series foundation model f_{θ^\dagger} pre-trained in Sec. 2.2.1 can be used in time-series classification and forecasting tasks. In general, there are two manners to apply the pretrained foundation model for the downstream tasks [63], i.e., *Partial Fine-Tuning (P-FT)* and *Full Fine-Tuning (F-FT)*. The main difference between P-FT and F-FT is the parameter size of the foundation models and decoders.

- **Partial Fine-Tuning (P-FT).** P-FT approaches [63, 72] are to keep the foundation model f_{θ^\dagger} frozen. They only train the decoder q_ϕ in downstream tasks. The objective is defined as follows.

$$\phi^* = \arg \min_{\phi} \mathcal{L}_{task}(q_\phi, f_{\theta^\dagger}, D_{task}) \quad (6)$$

- **Full Fine-Tuning (F-FT).** F-FT approaches [4, 7, 34, 59] involve training both the decoder q_ϕ and the foundation model f_{θ^\dagger} , encompassing parameters such as positional embeddings and LayerNorm parameters [7, 59], or the parameters within self-attention layers [4, 34] in downstream tasks, which is defined as follows.

$$\phi^*, \theta^* = \arg \min_{\phi} \mathcal{L}_{task}(q_\phi, f_{\theta^\dagger}, D_{task}) \quad (7)$$

Compared with P-FT, F-FT can optimize parameters of the foundation models for downstream tasks, expecting to achieve better performance than P-FT. Therefore, in this paper, we use F-FT to apply our model and baselines in the downstream tasks.

2.2.3 Variable independence. Many transformer-based learning models utilize the variable-mixing (or channel-mixing) configuration [69, 83], where the multivariate time-series $\mathbf{X} \in \mathbb{R}^{n \times T}$ is mapped into a timestamp-wise shared space $\mathbf{Z} \in \mathbb{R}^{T \times D}$ via an embedding layer. However, this approach introduces two critical issues: 1) The embedding layer requires the pre-definition of the

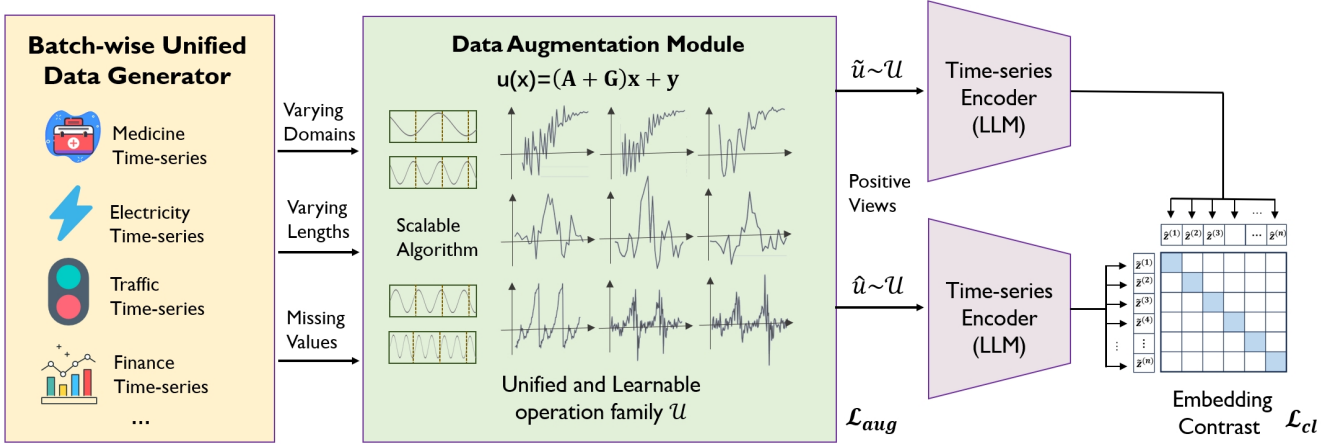


Figure 1: Overview of the UniCL

number of variables, which lacks generality for cross-domain pre-training; 2) A timestamp-wise shared embedding space may not be suitable for all domains, as the mechanism of dependency can vary (e.g., lag-features of financial time-series [53]). To facilitate universal pretraining, our study adopts the recent widely-adopted variable independence configuration [22, 43, 59], processing n variables independently.

3 FRAMEWORK OVERVIEW

In this study, we introduce UniCL, a universal contrastive learning framework designed for time-series analysis. UniCL is fundamentally general and effective, capable of handling heterogeneous cross-domain time-series data with varying input lengths, based on a unified augmentation operation that generates diverse positive samples, thereby facilitating robust contrastive learning.

We provide the overview of UniCL in Fig. 1. Primarily, there are four steps: (1) data generation, (2) unified and scalable data augmentation module, (3) time-series encoder based on LLMs, and (4) embedding contrast. Here, we briefly clarify these steps: (1) to begin with, the time-series datasets from diverse domains are initially partitioned into batches, shuffled, and then randomly fed into the augmentation module; (2) for each batch, the proposed scalable algorithm with bounded convergence loss can deal with varying lengths of inputs with missing values, and the unified and learnable augmentation operation is employed to generate diverse and pattern-preserved positive views for contrastive learning; (3) the CLIP-based encoder generates embeddings for all views, effectively capturing cross-domain and general time-series patterns; (4) a typical contrastive loss can be employed to enhance the discriminative power of the learned embeddings.

4 UNIFIED FOUNDATION MODEL

We first demonstrate our key observations about the bias in time-series representation caused by pre-determined augmentation methods. Then, we summarize existing methods and propose a unified and learnable augmentation operation family with theoretical guarantee. To facilitate the training of such operations, we introduce

two novel efficient loss functions. Additionally, we propose a scalable version of this unified operation set to handle datasets from various domains with different lengths and missing values. Finally, we introduce the encoder of the UniCL and the whole pre-training paradigm.

4.1 A Unified Data Augmentation Operation

4.1.1 Motivational observation of bias in embedding. As discussed in Sec. 1, existing pre-defined time-series augmentation methods introduce an **inductive bias** into representation learning amidst augmentation contrast. We present our key motivational observation: *the bias in time-series embedding correlates positively with the spectral distance (SD) between raw and augmented series*. To illustrate, we first quantify the bias introduced by the pre-defined data augmentation family $\mathcal{T}(\cdot)$ as follows, in line with a previous work [79]. Let $\{t^{(k)}(\mathbf{x}^{(j,i)})\}_{k=1}^K$ denotes the augmentation set of $\mathbf{x}^{(j,i)}$ with size K , where $t^{(k)} \sim \mathcal{T}$. Let $\mathcal{T}(\mathbf{x}^{(j,i)})$ symbolize the transformation distribution of $\mathbf{x}^{(j,i)}$. Then,

$$\begin{aligned} \text{Bias}(\mathcal{T}(\mathbf{x}^{(j,i)})) &= \left\| \mathbb{E}_{t \sim \mathcal{T}} [f_{\theta}(t(\mathbf{x}^{(j,i)}))] - f_{\theta}(\mathbf{x}^{(j,i)}) \right\|_2 \\ &\approx \left\| \frac{1}{K} \sum_{k=1}^K f_{\theta}(t^{(k)}(\mathbf{x}^{(j,i)})) - f_{\theta}(\mathbf{x}^{(j,i)}) \right\|_2 \end{aligned} \quad (8)$$

Let $\mathcal{F}(\cdot)$ denote the Fast Fourier Transform (FFT), and $|\cdot|$ denote the amplitude operator, which calculates the amplitude as $|\cdot| = \sqrt{\mathcal{R}(\cdot)^2 + \mathcal{I}(\cdot)^2}$, where $\mathcal{R}(\cdot)$ and $\mathcal{I}(\cdot)$ represent the real and imaginary part operators, respectively. Due to the conjugate symmetry of the frequency domain, we stipulate that the $|\cdot|$ operator only generates the first half and removes the zero-frequency component [68], i.e., $|\cdot| : \mathbb{C}^T \rightarrow \mathbb{R}^{\lfloor \frac{T}{2} \rfloor}$. Then, the spectral distance between $\mathbf{x}^{(j,i)}$ and $t(\mathbf{x}^{(j,i)})$ can be defined as:

$$SD(\mathbf{x}^{(j,i)}, t(\mathbf{x}^{(j,i)})) = \left\| |\mathcal{F}(\mathbf{x}^{(j,i)})| - |\mathcal{F}(t(\mathbf{x}^{(j,i)}))| \right\|_2^2 \quad (9)$$

We employ the representative and state-of-the-art contrastive learning method TS2Vec [72] to test 4 pre-defined augmentation

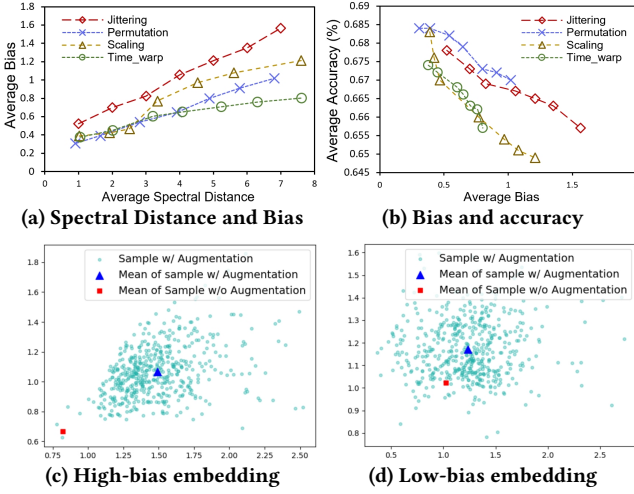


Figure 2: The bias observation of four pre-defined augmentation methods and each has seven variants. Fig. 1a illustrates the relationship between the average spectral distance of augmented and raw series and the average bias of learned embeddings. The y-axis represents bias, while the x-axis denotes the average spectral distance. Fig. 1b demonstrates the impact of embedding bias on downstream classification task. Here, the y-axis indicates the average accuracy, and the x-axis represents bias. Fig. 1c and Fig. 1d visualize the high-bias and low-bias of the embedding generated by the permutation.

methods on 23 selected multivariate datasets from the UEA Time Series Classification Archive [2] and report the average bias and spectral distance. For each dataset, we train the TS2Vec encoder with the same configuration as the original paper but varying the augmentation method. These methods encompass jittering, scaling, time warping, and permutation, each offering diverse variants achieved by adjusting hyper-parameters (e.g., the standard deviation of jittering). The output layer of the encoder has two dimensions to facilitate visualization. Following, we generate $K = 500$ augmented samples randomly for each sample, and compute the average bias $\frac{1}{mn} \sum_{j=1}^m \sum_{i=1}^n \text{Bias}(\mathcal{T}(\mathbf{x}^{(j,i)}))$ and the average spectral distance $\frac{1}{mnK} \sum_{j=1}^m \sum_{i=1}^n \sum_{k=1}^K SD(\mathbf{x}^{(j,i)}, t^{(k)}(\mathbf{x}^{(j,i)}))$, respectively. Fig. 2(a) illustrates a positive correlation between the average bias and the average spectral distance of augmented and raw series. Meanwhile, Fig. 2(b) demonstrates that greater bias in the embeddings results in reduced performance on downstream classification tasks. This observation motivates the need for time-series augmentation methods to control the spectral distance between augmented and raw time-series. As depicted in Fig. 2(c,d), within contrastive learning, a significant bias may hinder the effectiveness of separating augmented embeddings across different instances (e.g., $f_{\theta}(\tilde{\mathbf{x}}^{(j,i)}), \text{Neg}(\tilde{\mathbf{x}}^{(j,i)})$), thus limiting the discriminative power of learned embeddings for downstream tasks [79].

4.1.2 Unified Data Augmentation Operation. To mitigate the problem of inductive bias caused by pre-defined augmentation operation \mathcal{T} , one straightforward way is to employ all augmentation operations [39, 46, 78]. However, for some augmentation operations, the hyper-parameter space is continuous (e.g., standard deviation of jittering, number of speed changes of time warping), making it infeasible to explore the full augmented view space, especially

considering their compositions [46]. To address this challenge, we introduce a unified operation family \mathcal{U} . Formally, given input time-series $\mathbf{x}^{(j,i)}$, the augmentation operation u sampled from \mathcal{U} , i.e., $u \sim \mathcal{U}$, is defined as:

$$u(\mathbf{x}^{(j,i)}) = \mathbf{A}\mathbf{x}^{(j,i)} + \mathbf{y} \quad (10)$$

where $\mathbf{x}^{(j,i)} \in \mathbb{R}^T$, $\mathbf{A} \in \mathbb{R}^{T \times T}$ and $\mathbf{y} \in \mathbb{R}^T$. We provide Proposition 1 to demonstrate that the operation $u \sim \mathcal{U}$ yield an augmented view space equivalent to that of each pre-defined operation and their compositions.

Proposition 1. Existing time-series augmentation operation set \mathcal{T} includes jittering, scaling, magnitude warping, masking, pooling, and permutation. Then, the augmented view space of $\mathbf{x}^{(j,i)}$ generated by the unified operation $u \sim \mathcal{U}$ is the same as the view space generated by $t \sim \mathcal{T}$ as well as their compositions $\tilde{t} = t^{(n)} \circ t^{(n-1)} \circ \dots \circ t^{(1)}$, where $t^{(i)} \sim \mathcal{T}$.

PROOF. The proof for each augmentation operation is presented in Table 2. Therefore, for each $t^{(i)} \sim \mathcal{T}$, there exist matrix $\mathbf{A}^{(i)}$ and vector $\mathbf{y}^{(i)}$ such that $t^{(i)}(\mathbf{x}^{(j,i)}) = \mathbf{A}^{(i)}\mathbf{x}^{(j,i)} + \mathbf{y}^{(i)} \sim \mathcal{U}$. Let $\tilde{t} = t^{(n)} \circ t^{(n-1)} \circ \dots \circ t^{(1)}$ be the composite operator. Then,

$$\begin{aligned} \tilde{t}(\mathbf{x}) &= \mathbf{A}^{(n)} \cdot \left(\mathbf{A}^{(n-1)} \cdot \left(\dots \left(\mathbf{A}^{(1)}\mathbf{x}^{(j,i)} + \mathbf{y}^{(1)} \right) \dots \right) + \mathbf{y}^{(n-1)} \right) + \mathbf{y}^{(n)} \\ &= \mathbf{A}^{(n)} \cdot \mathbf{A}^{(n-1)} \dots \mathbf{A}^{(1)}\mathbf{x}^{(j,i)} + \sum_{i=2}^n \mathbf{A}^{(i)}\mathbf{y}^{(i-1)} + \mathbf{y}^{(n)} \\ &= \tilde{\mathbf{A}}\mathbf{x}^{(j,i)} + \tilde{\mathbf{y}} \end{aligned} \quad (11)$$

The above concludes that the compositions of t also belongs to the unified operation family \mathcal{U} . \square

Table 2: Proof of unified operation

Name	$t(\mathbf{x}^{(j,i)})$	$u(\mathbf{x}^{(j,i)}) = \mathbf{A}\mathbf{x}^{(j,i)} + \mathbf{y}$
Jittering	$\{x_k^{(j,i)} + \epsilon_k\}_{k=1}^T$, $\epsilon_k \sim \mathcal{N}(\mu, \sigma)$	$\mathbf{A} = \mathbf{I}, \mathbf{y} = (\epsilon_1, \dots, \epsilon_T)^T$
Scaling	$\{ax_k^{(j,i)}\}_{k=1}^T, a \in \mathbb{R}$	$\mathbf{A} = \text{Diag}\{a, \dots, a\}, \mathbf{y} = \mathbf{0}$
Magnitude warping	$\{a_k x_k^{(j,i)}\}_{k=1}^T, a_k \in \mathbb{R}$	$\mathbf{A} = \text{Diag}\{a_1, \dots, a_T\}, \mathbf{y} = \mathbf{0}$
Masking	$\{a_k x_k^{(j,i)}\}_{k=1}^T$, $a_k = \{0, 1\}$	$\mathbf{A} = \text{Diag}\{a_1, \dots, a_T\}, \mathbf{y} = \mathbf{0}$
Mean Pooling	The k -th bin = $\{\frac{1}{w} \cdot \sum_{h=w(k-1)+1}^{wk} x_h^{(j,i)}\}_w$	$\mathbf{A} = \begin{pmatrix} \mathbf{B} & \mathbf{0} \\ \mathbf{0} & \mathbf{B} \end{pmatrix}, \mathbf{B} = \frac{1}{w} \cdot \mathbf{1}_w$ $\mathbf{y} = \mathbf{0}$
Permutation	$\{x_{\pi(k)}^{(j,i)}\}_{k=1}^T$, $\pi \in S_T$	$\mathbf{A} = \begin{pmatrix} \mathbf{e}_{\pi(1)}^T \\ \vdots \\ \mathbf{e}_{\pi(T)}^T \end{pmatrix}, \mathbf{y} = \mathbf{0}$

To introduce randomness into the generation of diverse positive samples, without loss of generality, we can incorporate a random matrix \mathbf{G} with the deterministic matrix \mathbf{A} . Formally, given input time-series with length T , the **non-scalable unified operation** can be expressed as:

$$u(\mathbf{x}^{(j,i)}) = (\mathbf{A} + \mathbf{G})\mathbf{x}^{(j,i)} + \mathbf{y} \quad (12)$$

Algorithm 2: Non-scalable algorithm of unified operation

Input: Time-series $\mathbf{x}^{(j,i)} \in \mathbb{R}^T$, $T \times T$ Matrices \mathbf{A} , $\boldsymbol{\mu}^{(G)}$, $\boldsymbol{\sigma}^{(G)}$, T -dimension Vectors $\boldsymbol{\mu}^{(y)}$, $\boldsymbol{\sigma}^{(y)}$.

Output: The augmented time-series
// Generate Gaussian noise

```

1  $\mathbf{G}, \mathbf{y} \leftarrow \text{rand}(-1, 1)$ 
2  $\mathbf{G} \leftarrow \mathbf{G} \odot \boldsymbol{\sigma}^{(G)} + \boldsymbol{\mu}^{(G)}$ 
3  $\mathbf{y} \leftarrow \mathbf{y} \odot \boldsymbol{\sigma}^{(y)} + \boldsymbol{\mu}^{(y)}$ 
4 Return  $(\mathbf{A} + \mathbf{G})\mathbf{x}^{(j,i)} + \mathbf{y}$ 

```

and the matrix form is:

$$\mathbf{u}(\mathbf{X}^{(j)}) = \mathbf{X}^{(j)}(\mathbf{A} + \mathbf{G})^T + \mathbf{y} \quad (13)$$

where \mathbf{A} is a $T \times T$ deterministic matrix, \mathbf{G} is a $T \times T$ random matrix, and \mathbf{y} is a T dimensional random vector. As shown in Alg. 2, we set \mathbf{G} to be a Gaussian noise matrix (line 2), where all elements are independent and identically distributed (*i.i.d.*) random variable following Gaussian distribution, *i.e.*, $\mathbf{G}[i][j] \sim \mathcal{N}(\boldsymbol{\mu}^{(G)}[i][j], (\boldsymbol{\sigma}^{(G)}[i][j])^2)$. Here, both $\boldsymbol{\mu}^{(G)}$ and $\boldsymbol{\sigma}^{(G)}$ are $T \times T$ trainable matrix. Similarly, \mathbf{y} is a Gaussian noise vector (line 3), where all elements are *i.i.d.* and each y_i follows a Gaussian distribution $y_i \sim \mathcal{N}(\mu_i^{(y)}, (\sigma_i^{(y)})^2)$ with random vectors $\boldsymbol{\mu}^{(y)}$ and $\boldsymbol{\sigma}^{(y)}$ as trainable parameters. Therefore, the time and space complexity is $O(4T^2 + 3T)$, and we will introduce scalable and efficient algorithms in Section 4.2. Let $\mathcal{U}(\mathbf{x}^{(j,i)})$ symbolize the transformation distribution of $\mathbf{x}^{(j,i)}$, we have the following proposition:

Proposition 2. The transformation distribution $\mathcal{U}(\mathbf{x}^{(j,i)})$ follows a multivariate normal distribution.

PROOF. Considering the k -th random variable $(\mathcal{U}(\mathbf{x}^{(j,i)}))_k$, we have:

$$\begin{aligned} \mathcal{U}(\mathbf{x}^{(j,i)})_k &= (\mathbf{A}\mathbf{x}^{(j,i)})_k + (\mathbf{G}\mathbf{x}^{(j,i)})_k + y_k \\ &= (\mathbf{A}\mathbf{x}^{(j,i)})_k + \sum_{h=1}^T \mathbf{G}[k][h]x_h^{(j,i)} + y_k \end{aligned} \quad (14)$$

Notice that the first term is constant, as the matrix \mathbf{A} and input series $\mathbf{x}^{(j,i)}$ are deterministic. The remainder of the equation becomes a linear combination of normal distributions and *i.i.d.* random variables, *i.e.*, $\mathbf{G}[i][j]$ and y_k , resulting in $(\mathcal{U}(\mathbf{x}^{(j,i)}))_k$ following normal distribution. The above concludes that the transformation distribution $\mathcal{U}(\mathbf{x})$ is a multivariate normal distribution. \square

4.2 Scalable and Diverse Data Augmentation

We first propose a data augmentation objective based on our proposed unified operation to generate spectrum-preserved and diverse time-series data. Then, we propose a scalable algorithm to apply this objective to time-series data with various lengths.

4.2.1 A Spectrum-preserved and Diverse Objective. In contrastive learning, augmented data should satisfy two properties to be effective: pattern preservation and diversity [39]. Augmented data should preserve the essential pattern of the original data, ensuring that the similarity relationships between instances are maintained.

Then, the f_θ optimized by maximizing the similarity of positive views are expected to learn representations that capture time-series intrinsic patterns. Additionally, augmented data should introduce diversity into generated time-series, enabling the model to learn robust representations that generalize well to unseen data. We introduce two novel losses to facilitate the learning of our augmentation module: spectrum-preservation loss and spectrum-diversity loss.

1) Spectrum-preservation loss. As discussed in Sec. 4.1.1, in order to generate low-bias embeddings, the positive pairs $\tilde{\mathbf{x}}^{(j,i)}$ and $\hat{\mathbf{x}}^{(j,i)}$ should be close to the original series \mathbf{x} in terms of spectral distance. Therefore, the spectral distance in Eq. 9 can serve as the metric to measure the pattern differences of augmented series and raw series. Formally, the spectrum-preservation loss l_p can be defined as:

$$\begin{aligned} l_p(\mathcal{U}, \mathbf{x}^{(j,i)}) &= \frac{1}{2} \mathbb{E}_{\tilde{\mathbf{u}} \sim \mathcal{U}} [\|\mathcal{F}(\tilde{\mathbf{u}}(\mathbf{x}^{(j,i)})) - \mathcal{F}(\mathbf{x}^{(j,i)})\|_2^2] \\ &\quad + \frac{1}{2} \mathbb{E}_{\hat{\mathbf{u}} \sim \mathcal{U}} [\|\mathcal{F}(\hat{\mathbf{u}}(\mathbf{x}^{(j,i)})) - \mathcal{F}(\mathbf{x}^{(j,i)})\|_2^2] \\ &= \mathbb{E}_{\mathbf{u} \sim \mathcal{U}} [\|\mathcal{F}(\mathbf{u}(\mathbf{x}^{(j,i)})) - \mathcal{F}(\mathbf{x}^{(j,i)})\|_2^2] \end{aligned} \quad (15)$$

2) Spectrum-diversity loss. To enhance the diversity of the positive pairs $\tilde{\mathbf{x}}^{(j,i)}$ and $\hat{\mathbf{x}}^{(j,i)}$, we need to: **1)** define a metric to quantify the diversity of positive pairs, and **2)** identify which patterns in $\mathbf{x}^{(j,i)}$ are not essential and can therefore be diversified.

By Prop. 2, the positive pairs $\tilde{\mathbf{x}}^{(j,i)}$ and $\hat{\mathbf{x}}^{(j,i)}$ are two random vectors, where the k -th values $\tilde{x}_k^{(j,i)}$ and $\hat{x}_k^{(j,i)}$ are random variables with *i.i.d.* normal distribution. One intuitive approach to measure the diversity is to compute the average entropy of all random variables, given by $\frac{1}{T} \sum_{k=1}^T \ln(2\pi e \sigma_k^2)$, where $\sigma_k^2 = \sum_{h=1}^T (\boldsymbol{\sigma}^{(G)}[k][h])^2 x_h^{(j,i)} + (\sigma_k^{(y)})^2$. However, simply increasing the entropy of each point results in large $\boldsymbol{\sigma}^{(G)}$ and $\boldsymbol{\sigma}^{(y)}$, introducing meaningless noise. More generally, suppose the distribution of $\tilde{x}_k^{(j,i)}$ and $\hat{x}_k^{(j,i)}$ are unknown. Another intuitive approach to measure the diversity of positive views is to compute the average Kullback-Leibler (*KL*) divergence between the probability distributions of each pair of random variables at the same time point, given by $\frac{1}{T} \sum_{k=1}^T KL(P(\tilde{x}_k^{(j,i)}) || P(\hat{x}_k^{(j,i)}))$, where $P(\cdot)$ denotes the probability density function (PDF). However, in a time-series, only one observation is available at each timestamp. Estimating $P(\tilde{x}_k^{(j,i)})$ and $P(\hat{x}_k^{(j,i)})$ requires sampling $2M$ operators $\mathbf{u} \sim \mathcal{U}$, with M denoting the number of samplings for each view. Since this approximation must be conducted for every time point, the time complexity amounts to $O(2M \cdot T)$, which becomes infeasible when both M and T are large.

To tackle the complexity issue, rather than approximating the distribution in the time domain, we transform the positive views $\tilde{\mathbf{x}}^{(j,i)}$ and $\hat{\mathbf{x}}^{(j,i)}$ into the frequency domain as $|\mathcal{F}(\tilde{\mathbf{x}}^{(j,i)})|$ and $|\mathcal{F}(\hat{\mathbf{x}}^{(j,i)})|$, respectively. Here, the k -th element $|\mathcal{F}(\tilde{\mathbf{x}}^{(j,i)})|_k$ and $|\mathcal{F}(\hat{\mathbf{x}}^{(j,i)})|_k$, denoting the amplitude of the k -th frequency component, are also random variables. We convert the amplitude sequence to a probability mass function (PMF) by $P(\tilde{\mathbf{x}}^{(j,i)}) = \text{Softmax}(|\mathcal{F}(\tilde{\mathbf{x}}^{(j,i)})|/\tau)$ and $P(\hat{\mathbf{x}}^{(j,i)}) = \text{Softmax}(|\mathcal{F}(\hat{\mathbf{x}}^{(j,i)})|/\tau)$, where τ is the temperature parameter. Then, we can measure the diversity by calculating the Jensen-Shannon (*JS*) divergence between PMF $P(\tilde{\mathbf{x}}^{(j,i)})$ and PMF $P(\hat{\mathbf{x}}^{(j,i)})$, which is more efficient.

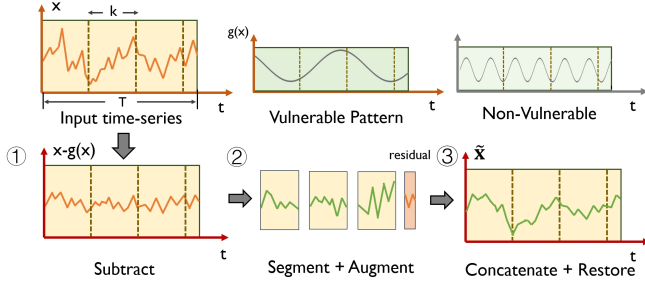


Figure 3: The procedure of the scalable algorithm involves augmenting time-series data with varying lengths through pattern-preserved segmentation and concatenation.

However, not all the frequency component should be diversified. Given $P(\tilde{\mathbf{x}}^{(j,i)}) = [\tilde{p}_1, \tilde{p}_2, \dots, \tilde{p}_{\lfloor \frac{T}{2} \rfloor}]$, the \tilde{p}_k represent the relative strength of k -th frequency within the entire spectrum. The low-frequency component ($k \rightarrow 1$) carries crucial semantic information such as trend and periodicity, while high-frequency component ($k \rightarrow \lfloor \frac{T}{2} \rfloor$) usually carries meaningless noise [83]. Therefore, we multiply the PMF by a decay factor $\alpha = [\alpha_1, \alpha_2, \dots, \alpha_{\lfloor \frac{T}{2} \rfloor}]^T$ using element-wise multiplication \odot , thereby assigning different weights to different components. Formally, the spectrum-diversity loss l_d can be defined as:

$$l_d(\mathcal{U}, \mathbf{x}^{(j,i)}, \alpha) = \mathbb{E}_{(\tilde{\mathbf{u}}, \hat{\mathbf{u}}) \sim \mathcal{U}} \left[-\log JS(\alpha \odot P(\tilde{\mathbf{u}}(\mathbf{x}^{(j,i)})) || \alpha \odot P(\hat{\mathbf{u}}(\mathbf{x}^{(j,i)}))) \right] \quad (16)$$

where $P(\cdot) = \text{Softmax}(|\mathcal{F}(\cdot)| / \tau)$, and \log is used to stabilize the optimization.

3) **Summary.** Formally, we define the objective function \mathcal{L}_{aug} of the data augmentation module as follows:

$$\mathcal{L}_{aug}(\mathcal{U}, \{\mathbf{X}^{(j)}\}_{j=1}^m, \alpha) = \sum_{j=1}^m \sum_{i=1}^n l_p(\mathcal{U}, \mathbf{x}^{(j,i)}) + \lambda \cdot l_d(\mathcal{U}, \mathbf{x}^{(j,i)}, \alpha) \quad (17)$$

where λ is a hyper-parameter.

4.2.2 Scalable operations. With the learnable unified operation and the corresponding loss function, the question is how we can efficiently employ it in time-series datasets exhibiting high variations, including varying sequence lengths and potential missing values.

1) **Varying sequence lengths.** To propose a scalable algorithm for handling inputs with varying lengths, two key issues need to be addressed: 1) Given the input series $\mathbf{x}^{(j,i)} \in \mathbb{R}^T$, the space complexity of the non-scalable algorithm outlined in Alg. 2 is $O(4 \times T^2 + 3T)$. This complexity becomes impractical when we receive the long sequence. 2) In large-scale pretraining, different datasets contain varying lengths of instances, and employing different size of unified operation for each dataset is inefficient. Thus, we introduce a scalable algorithm that offers efficient implementation, necessitating only a fixed-size unified operation across all datasets. This approach results in a space complexity of $O(K^2)$, where K is a constant.

Particularly, with a constant K , we define the **fix-sized unified operation** as follows:

Algorithm 3: Scalable algorithm of unified operation

Input: Time-series $\mathbf{x}^{(j,i)} \in \mathbb{R}^T$, Window size K , Linear function $g(\cdot)$, fix-sized unified operation $u \sim \mathcal{U}$.

Output: The augmented time-series

- 1 $\mathbf{x}^{(j,i)} \leftarrow \mathbf{x}^{(j,i)} - g(\mathbf{x}^{(j,i)})$
 - 2 $\mathbf{h}^{(1)}, \mathbf{h}^{(2)}, \dots, \mathbf{h}^{(\lfloor \frac{T}{K} \rfloor)} \leftarrow \mathbf{x}_{[1:K]}^{(j,i)}, \mathbf{x}_{[K+1:2K]}^{(j,i)}, \dots, \mathbf{x}_{[(\lfloor \frac{T}{K} \rfloor - 1) \cdot K + 1 : \lfloor \frac{T}{K} \rfloor \cdot K]}^{(j,i)}$
 - 3 $\mathbf{h}^{(\lfloor \frac{T}{K} \rfloor + 1)} \leftarrow \mathbf{x}_{[\lfloor \frac{T}{K} \rfloor \cdot K + 1 : T]}^{(j,i)}$
 - 4 $\{\tilde{\mathbf{h}}^{(1)}, \dots, \tilde{\mathbf{h}}^{(\lfloor \frac{T}{K} \rfloor)}\} \leftarrow \text{Augment} \{\mathbf{h}^{(1)}, \dots, \mathbf{h}^{(\lfloor \frac{T}{K} \rfloor)}\}$ separately using $\tilde{\mathbf{u}} \sim \mathcal{U}$ in Eq. 18.
 - 5 $\tilde{\mathbf{x}}^{(j,i)} \leftarrow \text{concatenate} [\tilde{\mathbf{h}}^{(1)}, \dots, \tilde{\mathbf{h}}^{(\lfloor \frac{T}{K} \rfloor)}, \mathbf{h}^{(\lfloor \frac{T}{K} \rfloor + 1)}]$
 - 6 $\tilde{\mathbf{x}}^{(j,i)} \leftarrow \tilde{\mathbf{x}}^{(j,i)} + g(\mathbf{x}^{(j,i)})$
 - 7 **Return** $\tilde{\mathbf{x}}^{(j,i)}$
-

$$u(\mathbf{x}^{(j,i)}, k) = (\mathbf{A}_{k \times k} + \mathbf{G}_{k \times k}) \mathbf{x}_{k \times 1}^{(j,i)} + \mathbf{y}_{k \times 1} \quad (18)$$

Such an operation can only handle input time-series with a fix length K , therefore we need to extend (resp. segment) the inputs $\mathbf{x}^{(j,i)}$ when $T < K$ (resp. $T > K$). When $T < K$, we employ iterative extension of the time series through repetition until its length equals K . This iterative repetition aligns with the periodicity assumption of Fourier analysis, ensuring $x_i = x_{i+T}$, thereby preserving the amplitude spectrum of \mathbf{x} . Conversely, alternative methods such as padding [74] may disrupt the spectrum pattern of \mathbf{x} .

As illustrated in Fig. 3 and Alg. 3, when $T > K$, we employ segmentation to the input time-series. Since segmentation may disrupt the intrinsic pattern, we first denote the $g(\mathbf{x})$ as the vulnerable pattern which will be disrupted by segmentation. This pattern should be subtracted prior to the segmentation (line 1) and restored after concatenation (line 6), which is spectrum-preservation due to the linearity of the Fourier transform. Then, we segment the time-series into $\lfloor \frac{T}{K} \rfloor + 1$ non-overlapping and contiguous subseries $\{\mathbf{h}^{(l)} \in \mathbb{R}^K, \mathbf{h}^{(l \cdot \frac{T}{K} + 1)} | l = 1, \dots, \lfloor \frac{T}{K} \rfloor\}$ (line 2), where $\mathbf{h}^{(\lfloor \frac{T}{K} \rfloor + 1)} \in \mathbb{R}^{res}$ is the residual term and $0 \leq res < K$. Subsequently, we augment each subseries separately using fix-sized unified operation (line 4) and concatenate them in the same order as $\tilde{\mathbf{x}}^{(j,i)} = [\tilde{\mathbf{u}}^{(1)}(\mathbf{h}^{(1)}, k), \dots, \tilde{\mathbf{u}}^{(\lfloor \frac{T}{K} \rfloor)}(\mathbf{h}^{(\lfloor \frac{T}{K} \rfloor)}, k), \mathbf{h}^{(\lfloor \frac{T}{K} \rfloor + 1)}]$, where $\tilde{\mathbf{u}} \sim \mathcal{U}$. Finally, we obtain the augmented series by restoration (line 6).

Time and Space Complexity. For line 1-3 and 5-6, the time and space complexity is $O(4T)$. For line 4, since only a fix-sized unified operation family is needed, the space complexity is $O(4K^2 + 3K)$ according to Alg. 2 and the time complexity is $O(\lfloor \frac{T}{K} \rfloor \cdot (4K^2 + 3K))$.

Proposition 3. Given that 1) $K < T$; 2) $g(\mathbf{x}^{(j,i)})$ is a linear function (i.e., a linear map $g: \mathbb{R}^T \mapsto \mathbb{R}^T$): then the augmented view space generated by the scalable algorithm Alg. 3 is a subspace of the view space generated by the non-scalable algorithm Alg. 2.

PROOF. We can express the equivalent form of the scalable algorithm by introducing a **scalable unified operation** family \mathcal{S} . For each scalable unified operation $s \sim \mathcal{S}$, we have:

$$s(\mathbf{x}^{(j,i)}, k) = (\mathbf{A}'_{T \times T} + \mathbf{G}'_{T \times T}) \cdot (\mathbf{x}^{(j,i)} - g(\mathbf{x}^{(j,i)})) + \mathbf{y}'_{T \times 1} + g(\mathbf{x}^{(j,i)}) \quad (19)$$

where $\mathbf{A}'_{T \times T} = \text{Diag}\{\mathbf{A}_{k \times k}^{(1)}, \dots, \mathbf{A}_{k \times k}^{(\lfloor \frac{T}{K} \rfloor)}, \mathbf{I}_{res \times res}\}$ and $\mathbf{G}'_{T \times T} = \text{Diag}\{\mathbf{G}_{k \times k}^{(1)}, \dots, \mathbf{G}_{k \times k}^{(\lfloor \frac{T}{K} \rfloor)}, \mathbf{I}_{res \times res}\}$ are both block diagonal matrices, and $\mathbf{y}'_{T \times 1} = [(\mathbf{y}_{k \times 1}^{(1)})^T \dots, \mathbf{1}_{res \times 1}^T]^T$. Since $g(\mathbf{x}^{(j,i)})$ is a linear function, we have $g(\mathbf{x}^{(j,i)}) = \mathbf{H}\mathbf{x}^{(j,i)}$, where \mathbf{H} is a $T \times T$ matrix. Thus, we get the following Equation:

$$\begin{aligned} s(\mathbf{x}^{(j,i)}, k) &= (\mathbf{A}'_{T \times T} + \mathbf{G}'_{T \times T}) \cdot (\mathbf{x}^{(j,i)} - \mathbf{H}\mathbf{x}^{(j,i)}) + \mathbf{y}'_{T \times 1} + \mathbf{H}\mathbf{x}^{(j,i)} \\ &= ((\mathbf{A}'_{T \times T} (\mathbf{I} - \mathbf{H}) + \mathbf{H}) + (\mathbf{G}'_{T \times T} (\mathbf{I} - \mathbf{H}))) \mathbf{x}^{(j,i)} + \mathbf{y}'_{T \times 1} \\ &= (\mathbf{A}^{new} + \mathbf{G}^{new}) \mathbf{x}^{(j,i)} + \mathbf{y}^{new} \sim \mathcal{U} \end{aligned} \quad (20)$$

Thus, we have $\mathcal{S} \subset \mathcal{U}$. \square

LEMMA 4.1. *The difference in loss convergence between scalable and non-scalable algorithms is bounded by: (1) hyperparameter λ ; (2) the spectral distance $SD(s(\mathbf{x}, k), u(\mathbf{x}, T))$, where $s \sim \mathcal{S}, u \sim \mathcal{U}$.*

PROOF. By Prop. 3, the non-scalable operation $u \sim \mathcal{U}$ is associated with a larger hypothesis space compared to the scalable operation $s \sim \mathcal{S}$. Without loss of generality, we make the assumption that $\mathcal{L}_{aug}(\mathcal{U}^*, \{\mathbf{X}^{(j)}\}_{j=1}^m, \alpha) < \mathcal{L}_{aug}(\mathcal{S}^*, \{\mathbf{X}^{(j)}\}_{j=1}^m, \alpha)$, where $\mathcal{U}^* = \arg \min_{\mathcal{U}} \mathcal{L}_{aug}(\mathcal{U}, \{\mathbf{X}^{(j)}\}_{j=1}^m, \alpha)$ and $\mathcal{S}^* = \arg \min_{\mathcal{S}} \mathcal{L}_{aug}(\mathcal{S}, \{\mathbf{X}^{(j)}\}_{j=1}^m, \alpha)$. We derive the upper bound of the difference of the convergence loss:

$$\begin{aligned} &|\mathcal{L}_{aug}(\mathcal{S}^*, \{\mathbf{X}^{(j)}\}_{j=1}^m, \alpha) - \mathcal{L}_{aug}(\mathcal{U}^*, \{\mathbf{X}^{(j)}\}_{j=1}^m, \alpha)| \\ &= \mathcal{L}_{aug}(\mathcal{S}^*, \{\mathbf{X}^{(j)}\}_{j=1}^m, \alpha) - \mathcal{L}_{aug}(\mathcal{U}^*, \{\mathbf{X}^{(j)}\}_{j=1}^m, \alpha) \\ &= \sum_{j=1}^m \sum_{i=1}^n l_p(\mathcal{S}^*, \mathbf{x}^{(j,i)}) - l_p(\mathcal{U}^*, \mathbf{x}^{(j,i)}) + \lambda l_d(\mathcal{S}^*, \mathbf{x}^{(j,i)}, \alpha) - \\ &\quad \lambda l_d(\mathcal{U}^*, \mathbf{x}^{(j,i)}, \alpha) \\ &\leq \sum_{j=1}^m \sum_{i=1}^n l_p(\mathcal{S}^*, \mathbf{x}^{(j,i)}) - l_p(\mathcal{U}^*, \mathbf{x}^{(j,i)}) + \lambda \cdot \ln 2 \\ &= \sum_{j=1}^m \sum_{i=1}^n \mathbb{E}_{s \sim \mathcal{S}^*} [\|F(s(\mathbf{x}^{(j,i)})) - F(\mathbf{x}^{(j,i)})\|_2^2] - \\ &\quad \mathbb{E}_{u \sim \mathcal{U}^*} [\|F(u(\mathbf{x}^{(j,i)})) - F(\mathbf{x}^{(j,i)})\|_2^2] + \lambda \cdot \ln 2 \end{aligned} \quad (21)$$

Therefore, to lower the upper bound, we can 1) choose small λ ; 2) choose $g(\cdot)$ by optimizing the below optimization problem:

$$g^* = \arg \min_g \sum_{j=1}^m \sum_{i=1}^n \mathbb{E}_{s \sim \mathcal{S}^*, u \sim \mathcal{U}^*} \|SD(s(\mathbf{x}^{(j,i)}, k), u(\mathbf{x}^{(j,i)}, T))\|_2^2 \quad (22)$$

\square

The Lemma 4.1 suggests that the augmented time-series generated by scalable operation $s \sim \mathcal{S}$ and non-scalable operation $u \sim \mathcal{U}$ should exhibit small spectral distance. However, in Alg. 3, segmenting the time-series into K non-overlapping subseries may disrupt the $\lfloor \frac{T}{K} \rfloor$ lowest frequency components. Therefore, we define the linear function $g(\cdot)$ to extract the lowest $\lfloor \frac{T}{K} \rfloor$ frequency

components, thereby preserve such vulnerable patterns. The k -th value of function $g(\cdot)$ can be formulated as:

$$g(\mathbf{x}^{(j,i)})[k] = \sum_{h=0}^{\lfloor \frac{T}{K} \rfloor} 2 \cdot amp_h \cdot \cos(2\pi f_h(k-1) + \phi_h) \quad (23)$$

where $h = 1, 2, \dots, T$, amp_h is the amplitude, f_h is the angular frequency, and ϕ_h is the phase of the h -th lowest frequency component.

2) **Missing values.** Given a minibatch $\{\mathbf{X}^{(j)}\}_{j=1}^m$ of time-series data, which may contain missing values requiring imputation, we are motivated by the recognition that the low-frequency components carry essential information, while the high-frequency components often introduce noise. To address this, we initially employ linear interpolation to handle missing values in $\mathbf{X}^{(j)}$. Subsequently, to filter out the high-frequency noise introduced by linear interpolation, we apply a moving average with a window size of 10.

4.2.3 Training algorithm. We summarize the learning objectives and scalable algorithm of the data augmentation module in Algorithm 4. To calculate the expectations in Eq.15 and Eq.16, we introduce two hyper-parameters, denoted as C_1 and C_2 . Here, C_1 represents the number of samplings for the unified operations in the spectrum-preservation loss (line 8), and C_2 is the number of sampled operation pairs in the spectrum-diversity loss (line 14), where $C_2 \leq \binom{C_1}{2}$. The outcomes of parameter-sensitive experiments are presented in Sec. 5.4. Empirically, employing small values for C_1 and C_2 has demonstrated both efficiency and effectiveness.

Time complexity. The time complexity of Alg. 4 is analyzed as follows. Assuming the length of each time-series is denoted as T , the loop from lines 2 to 16 takes $O(m)$ time to traverse all input time-series. Lines 3 to 4 perform linear interpolation and moving average with a small constant window size, which takes $O(T)$ time. Line 8 involves a scalable operation comprising matrix multiplication and addition operations based on Eq. 13 and Eq. 19. Let the fixed window length be denoted as K , then the time complexity is $O(\lfloor \frac{T}{K} \rfloor \cdot n \cdot (4K^2 + 3K)) \approx O(T \cdot n \cdot K)$ according to Alg. 3. Line 10 can be computed using the fast Fourier transform (FFT), which takes $O(n \cdot T \cdot \log T)$ time. Line 13 is not counted since C_1 is a small constant. Line 14 reuses the results from line 8 and aims to calculate the JS divergence, which takes $O(n \cdot T)$ time. Thus, the total time complexity of Algorithm 4 is $O(mT + mnC_1 \cdot T \cdot K + mnC_1 \cdot T \log T + mnC_2 \cdot T)$. In practice, as m represents the number of time-series and n represents the number of variables, both can be organized into a single matrix to leverage GPU resources for accelerated computation.

4.3 Pre-train LLM

4.3.1 Encoder design. The encoder f_θ comprises two primary components: an input embedding layer and a stack of causal transformer-encoder blocks. Initially, the input embedding layer partitions the input positive views $\tilde{\mathbf{X}}^{(j)}$ and $\hat{\mathbf{X}}^{(j)}$ generated by the augmentation module into a series of consecutive patches, which may be overlapping or non-overlapping [43], each with a length of L_p . The total count of patches is $P = \lfloor \frac{(T-L_p)}{S} \rfloor + 1$, where S represents the sliding stride. Subsequently, a reprogramming layer [34] is employed to transform the $\tilde{\mathbf{X}}_p^{(j)}, \hat{\mathbf{X}}_p^{(j)} \in \mathbb{R}^{n \times P \times L_p}$ into the high-dimensional

Algorithm 4: The training algorithm of the data augmentation module by using scalable algorithm.

Input: A batch $D_{batch} = \{X^{(j)}\}_{j=1}^m$, the scalable augmentation family \mathcal{S} , number of samplings C_1 and C_2 , where $C_2 \leq \binom{C_1}{2}$

Output: The batch loss \mathcal{L}_{aug}

```

1  $\mathcal{L}_{aug} \leftarrow 0$ 
2 for each  $X^{(j)} \in D_{batch}$  do
3   if has missing then
4      $X^{(j)} \leftarrow \text{Moving\_Average}(\text{Interpolation}(X^{(j)}))$ 
5    $l_p, l_d, \text{aug\_list} \leftarrow 0, \phi$ 
6   for  $k = 1$  to  $C_1$  do
7     draw scalable operation  $s^{(k)} \sim \mathcal{S}$ 
8      $\hat{X}^{(j)} \leftarrow s^{(k)}(X^{(j)})$  // Matrix form Eq. 13
9      $\text{aug\_list}[k] \leftarrow \hat{X}^{(j)}$ 
10     $l_p \leftarrow l_p + \frac{1}{n} \sum_{i=1}^n \|\mathcal{F}(\hat{x}^{(j,i)})\| - \|\mathcal{F}(x^{(j,i)})\|^2_2$ 
11     $l_p \leftarrow l_p / C_1$ 
12    // Sampling for the diversity loss
13    for  $k = 1$  to  $C_2$  do
14      // Sampling two indices  $\binom{|C_1|}{2}$ 
15       $(idx_1, idx_2) \leftarrow \text{Sampling\_pairs}(C_1)$ 
16       $l_d \leftarrow l_d + \frac{1}{n} \sum_{i=1}^n -\log JS(\alpha \odot P(\text{aug\_list}[idx_1][i]) || \alpha \odot P(\text{aug\_list}[idx_2][i]))$ 
17     $l_d \leftarrow l_d / C_2$ 
18     $\mathcal{L}_{aug} = \mathcal{L}_{aug} + l_p + \lambda \cdot l_d$ 
19 Return  $\frac{1}{m} \mathcal{L}_{aug}$ 

```

space $\tilde{H}_p^{(j)}, \hat{H}_p^{(j)} \in \mathbb{R}^{n \times P \times D}$. Then, both $\tilde{H}_p^{(j)}$ and $\hat{H}_p^{(j)}$ are fed into the causal transformer-decoder blocks for representation learning, which mirror the architecture of the text encoder in ViT-G/14 CLIP, comprising 32 transformer blocks with 1280 hidden dimensions. The weights of these 32 blocks are initialized from ViT-G/14 CLIP as well. ViT-G/14 CLIP is a large pre-trained model designed for processing visual and textual data, trained on approximately 400M pairs of text and images using contrastive learning. We opt for ViT-G/14's text encoder structure due to our shared contrastive-based pre-training paradigm and mutual need for sequence modeling. The output of the encoder is the patch-wise embeddings, denoted as $\tilde{Z}^{(j)}, \hat{Z}^{(j)} \in \mathbb{R}^{n \times P \times D}$. In summary, the encoder can be represented as a mapping function $f_\theta : \mathbb{R}^{n \times T} \rightarrow \mathbb{R}^{n \times P \times D}$.

4.3.2 Contrastive Loss. We leverage the hierarchical contrastive loss \mathcal{L}_{cl} introduced by TS2Vec [72], which contrasts learned embeddings at different scales, thereby enhancing fine-grained representation learning for a variety of downstream tasks.

4.3.3 Pre-training paradigm. In the large-scale pre-training, the encoder f_θ is trained in a wide range of time-series data from various domains, denoted as $D_{train} = \{D_1, D_2, \dots, D_N\}$. However, training sequentially (i.e., $D_1 \rightarrow D_2 \rightarrow \dots \rightarrow D_N$) may lead to catastrophic forgetting problem [18]. To overcome this problem, we preprocess all the time-series data into batches, $D_i \rightarrow \{batch_1^{(i)}, batch_2^{(i)}, \dots\}$, where each batch from different domains contain varying length

Algorithm 5: The pre-training paradigm of UniTS.

Input: Shuffled datasets $D_{train} = \{D_{batch}^{(k)}\}_{k=1}^N$, the scalable augmentation family \mathcal{S} , the encoder f_θ , epoch number E_1, E_2 , and E_3 , learning rate η_1 and η_2

Output: The encoder f_{θ^*} and the decoder q_{ϕ^*}

```

1 for  $i = 1$  to  $E_1$  do
2   for each  $D_{batch} \in D_{train}$  do
3     for  $i = 1$  to  $E_2$  do
4       // Data augmentation module in Alg. 4
5        $\mathcal{L}_{aug} \leftarrow \text{scalable\_algorithm}(D_{batch}, \mathcal{S})$ 
6        $\theta_S \leftarrow \theta_S - \eta_1 \nabla_{\theta_S}(\mathcal{L}_{aug})$ 
7     for  $i = 1$  to  $E_3$  do
8       // Updates encoder  $f_\theta$ 
9        $\mathcal{L}_{cl} \leftarrow f_\theta(D_{batch})$ 
10       $\theta_f \leftarrow \theta_f - \eta_2 \nabla_{\theta_f}(\mathcal{L}_{cl})$ 
11 Return the trained operations  $\mathcal{S}^*$  and trained encoder  $f_{\theta^*}$ 

```

of time-series data. During training, we shuffle batches across all domains to improve the robustness and generality of the learned encoder. Instead of optimizing the augmentation module and encoder simultaneously, We train alternatively as described in Alg. 5. Such approach can effectively tackle the complex optimization problems and avoid problems such as asynchronous optimization. Specifically, for each batch of data, we iteratively train the data augmentation module for E_1 iterations, followed by training the encoder for E_2 iterations with the augmentation module held fixed.

The time complexity of Alg. 5 is $O(N \cdot E_1 \cdot E_2)$, and the results of parameter-sensitive experiments are presented in Sec. 5.4. Empirically, employing small values for E_1 and E_2 has demonstrated both efficiency and effectiveness.

5 EXPERIMENTS

We evaluate our approach across a diverse set of time-series analysis tasks, as outlined in Sec. 2, encompassing time-series forecasting and time-series classification. Our comparative study encompasses a comprehensive range of state-of-the-art models, including supervised models and foundational time-series models. Moreover, we conduct additional ablation analyses to assess the scalability and efficacy of the proposed data augmentation methods.

5.1 Experiment Settings

5.1.1 Datasets. In our study, we assess the effectiveness of our model, UniCL, across a diverse array of datasets for various time-series analysis tasks. To ensure fair comparison, we adhere to the experimental settings established in TimesNet [68]. For time-series forecasting, we utilize seven well-established real-world datasets: four ETT datasets [82] (ETTh1, ETTh2, ETTm1, ETTm2), Weather¹, Electricity², and ILI³. For time-series classification, we evaluate the performance across ten multivariate UEA classification datasets [2].

¹<https://www.bgc-jena.mpg.de/wetter/>

²<https://archive.ics.uci.edu/ml/datasets/ElectricityLoadDiagrams20112014>

³<https://gis.cdc.gov/grasp/fluview/fluportal/dashboard.html>

Table 3: Time-series forecasting tasks. The results are averaged from 4 different prediction lengths, that is {24, 36, 48, 60} for ILI and {96, 192, 336, 720} for the others. We bold the best performance among LLM-based models, which is on the left-hand side of the two vertical lines. We highlight the best performance for the entire row by both bolding and underlining it.

Methods	UniCL		TimeLLM [†]		GPT4TS		LLaTA [†]		UniTime [†]		TimesNet		PatchTST		LightTS		DLinear	
	MSE	MAE	MSE	MAE	MSE	MAE	MSE	MAE	MSE	MAE	MSE	MAE	MSE	MSE	MAE	MSE	MAE	MSE
ETm1	<u>0.343</u>	<u>0.372</u>	0.357	0.380	0.352	0.383	0.364	0.379	0.372	0.386	0.400	0.406	0.351	0.387	0.435	0.437	0.357	0.378
ETm2	0.271	0.325	0.269	0.335	0.266	0.326	0.278	0.334	0.283	0.339	0.291	0.333	0.255	0.315	0.409	0.436	0.267	0.334
ETTh1	0.422	0.420	0.432	0.435	0.427	0.426	0.425	0.423	0.435	0.429	0.458	0.450	0.413	0.430	0.491	0.497	0.423	0.437
ETTh2	0.334	0.378	0.349	0.393	0.346	0.394	0.342	0.389	0.352	0.395	0.414	0.427	0.330	0.379	0.602	0.543	0.431	0.447
ECL	0.160	0.257	0.173	0.269	0.167	0.263	0.162	0.256	0.181	0.282	0.192	0.295	0.161	0.253	0.229	0.329	0.166	0.263
Weather	0.227	0.264	0.245	0.277	0.237	0.270	0.231	0.273	0.245	0.279	0.259	0.287	0.225	0.264	0.261	0.312	0.249	0.300
ILI	1.912	0.891	1.937	0.915	1.925	0.903	1.931	0.908	2.270	1.040	2.139	0.931	1.443	0.798	7.382	2.003	2.169	1.041
Average	0.524	0.415	0.537	0.429	0.531	0.424	0.533	0.423	0.591	0.450	0.593	0.447	0.454	0.404	1.401	0.651	0.573	0.457

[†] means that we modify the official code (e.g., modify the input embedding layer) for fair comparison.

5.1.2 Baselines. We thoroughly compare our approach against a wide-range of time-series models, including the followings: (1) Transformer-based supervised models: ETSformer [67], FEDformer [83], PatchTST [43], Autoformer [69], Informer, Non-stationary Transformer [38], and Flowformer [20]; (2) Other supervised models: TimesNet [68], LightTS [77], DLinear [73], TCN [15], XGBoost [5], LSTNet [27], and Rocket [10]; (3) LLM-based time-series foundation models: Time-LLM [22], GPT4TS [59], UniTime [36], and LLaTA [34].

5.1.3 Implementation details. With the aid of the scalable algorithm, UniCL undergoes initial pre-training on 40 cross-domain datasets sourced from the Monash Time Series Forecasting Repository [17]. These datasets encompass data with varying lengths, ranging from 2 to 7M, and include instances with missing values, with missing rate ranging from 2% to 17%. It should be notice that the training data in the experiments is not involved. We pre-train our model on four NVIDIA A800 GPU for one week. Specifically, the ViT-G/14 Clip encoder utilizes a layer count of 32, with attention blocks fine-tuned using LoRA [19]. Other parameters are also fine-tuned during pretraining. The fixed window size k of the scalable algorithm is set to 120, while E_1 and E_2 in Alg.5 are configured as 3 and 1 respectively. The values of C_1 and C_2 in Alg. 4 are chosen as 5 and 2 respectively, and λ in Eq. 17 is set to 0.01. Both the augmentation module and the encoder are trained using the AdamW optimizer with an initial learning rate of 0.0001. After pre-training, we integrate our trained encoder into the existing pipeline⁴ for evaluation. We also adhere to the same experimental settings as in Wu et al. [68] for all tasks.

5.2 Main Experiments

5.2.1 Time-series forecasting. Time-series forecasting tasks involve prediction horizons ranging from 24 to 720, with evaluation metrics including mean square error (MSE) and mean absolute error (MAE). Tab. 3 presents a comprehensive overview of the experimental findings. We utilize two vertical lines to demarcate the table. The right part of the table represents state-of-the-art supervised learning models, while the left part pertains to LLM-based time-series foundation models that leverage natural language knowledge for

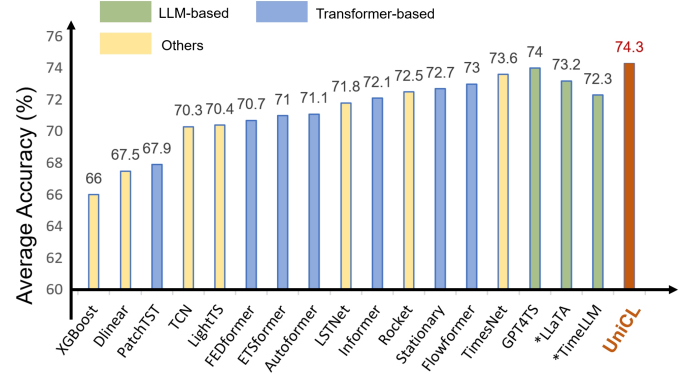


Figure 4: Results of time-series classification tasks. The accuracy is averaged from 10 subsets of UEA. * means that we modify the baseline’s code (e.g., modify the output layer for classification). Other results are from GPT4TS [59].

time-series analysis. UniCL exhibits superior performance across two evaluation criteria, surpassing all LLM-based time-series foundation models. Notably, UniCL outperforms the state-of-the-art LLM-based model GPT4TS, resulting in a notable 1.3% average reduction in MSE and a 2.1% average reduction in MAE. UniCL demonstrates competitive results when compared to the supervised models PatchTST, significantly bridging the gap between foundation models and supervised models.

5.2.2 Time-series classification. As depicted in Fig. 4, UniCL attains an average accuracy of 74.3%, surpassing all baseline methods across 10 multivariate UEA datasets. Notably, UniCL outperforms the state-of-the-art forecasting models TimeLLM and LLaTA by approximately 1%, while also surpassing the previous state-of-the-art transformer-based models PatchTST by 5.8%. The superior performance of UniCL may be attributed to the good generality of contrastive learning, which effectively discriminates between diverse and unseen positive and negative views.

5.3 Ablation Study

5.3.1 Ablation on the losses and unified operations. To better understand the effectiveness of the data augmentation module designs in UniCL, a comparison between full UniCL and its 8 variants

⁴<https://github.com/thuml/Time-Series-Library>

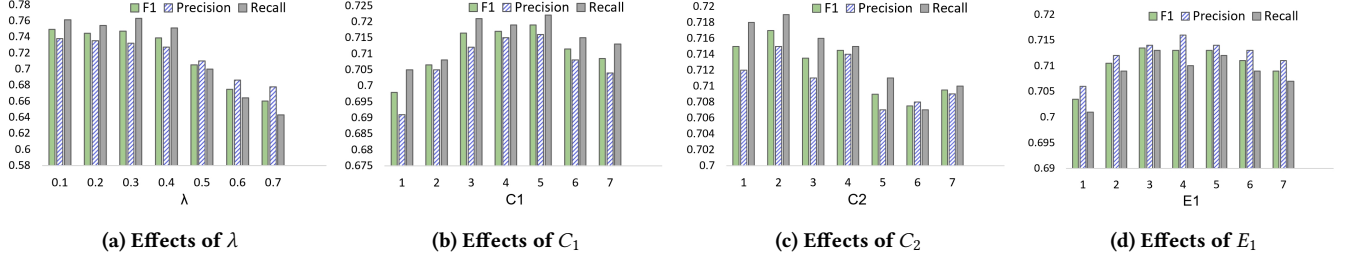


Figure 5: Parameter sensitivity evaluation. When testing C_1 , we fix $C_2 = 2$, and when testing C_2 , we fix $C_1 = 3$.

on 128 UCR datasets [9] is shown in Tab. 4, where 1) **w/o Spectrum-Preservation Loss** removes the spectrum-preservation loss; 2) **w/o Spectrum-Diversity Loss** removes the spectrum-diversity loss; 3) **Unified operation** $\rightarrow X$: replaces our proposed unified and learnable operation into 6 different pre-defined augmentation strategies, including jittering, scaling, permutation, masking, pooling, and warping. We observe a significant drop in performance when removing the Spectrum-Preservation Loss, suggesting that by learning spectrum-preserved patterns, the model can effectively capture important patterns within the time-series data. The absence of Spectrum-Diversity Loss resulted in a notable decrease in accuracy, amounting to 9.2%. This underscores the importance of diverse positive views for ensuring the discriminative power of learned embeddings. Furthermore, decreased performance is observed across all augmentation-based variants, with reductions ranging from 2.1% (masking) to 6.1% (scaling). The relatively minor decrease in performance observed with jittering and masking may be attributed to their ability to generate spectrum-preserved and diverse samples. In summary, the full UniCL leads to the best performance.

Table 4: Ablation study on 128 UCR datasets. The results are averaged from 128 time-series classification tasks.

		Avg. Accuracy
Full UniCL		0.844
Loss	w/o Spectrum-Preservation Loss	0.710(−13.4%)
	w/o Spectrum-Diversity Loss	0.752(−9.2%)
Augment- ation	Unified operation \rightarrow Jittering	0.815(−2.9%)
	Unified operation \rightarrow Scaling	0.783(−6.1%)
	Unified operation \rightarrow Permutation	0.794(−5.0%)
	Unified operation \rightarrow Masking	0.823(−2.1%)
	Unified operation \rightarrow Pooling	0.810(−3.4%)
	Unified operation \rightarrow Warping	0.818(−2.6%)

5.3.2 Ablation on the scalable algorithm. To better understand the role of the scalable algorithm designs in UniCL, we evaluate the efficiency of the scalable operations and non-scalable operations, as illustrated in Fig. 6(a). The experiment is conducted on synthetic time-series data with varying lengths, and the time cost per epoch and final average is recorded. We observe that beyond a length of 300, the time cost of non-scalable operations increases exponentially, whereas the time cost of scalable operations remains linear with the length of the input. This is due to the design of the scalable algorithm. To demonstrate the effectiveness of the scalable algorithm, the corresponding convergence losses of Fig. 6(a) are

illustrated in Fig. 6(b). Despite the significantly lower time consumption of scalable operations compared to non-scalable ones, we observe that the difference in convergence loss between scalable and non-scalable operations is bounded.

5.4 Parameter Sensitivity

We evaluate the performance of the UniCL based on different parameters: λ in Eq. 17, C_1, C_2 in Alg. 4, and E_1 in Alg. 5. The experiment is conducted on two anomaly detection datasets: Yahoo [44] and KPI [54], following an evaluation protocol [54]. As demonstrated in Fig. 5(a), the F1 metric drops with λ larger than 0.4, suggesting that a wise selection of λ should be less than 0.4, which is consistent with Lemma 4.1. According to Fig. 5(b,c), the wise selection for C_1 and C_2 falls within the range of 3 to 5 and 1 to 3, respectively, underscoring the importance of the spectrum-preserved property over the spectrum-diverse property. Furthermore, the choice of E_1 holds critical importance in alternative training, with the results indicating that E_1 should fall within the range of 3 to 6. A smaller value of E_1 may result in underfitting of the augmentation module.

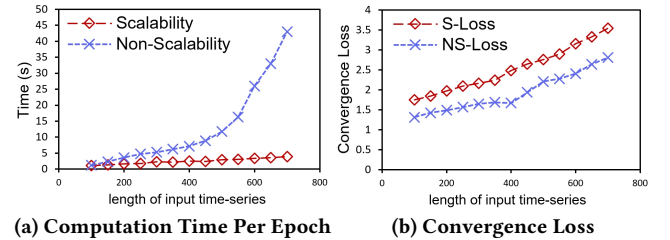


Figure 6: Efficiency estimation regarding the length of the input time-series and its effect on the corresponding convergence loss. The window size of the scalable algorithm is set to 100. S-Loss refers to the convergence loss of the scalable operation and NS-Loss refers to the convergence loss of the non-scalable operation.

6 CONCLUSION

In this paper, we propose UniCL, a universal contrastive learning framework for pre-training time series models across diverse domains, which addresses the limitations of high bias and low generality in existing models. First, we propose a novel augmentation operation that preserves spectral properties, ensuring diversity and reduced bias in augmented time-series data. Second, we propose a scalable augmentation algorithm to time series data with high variability in terms of domain, sequence length, and variable number, thus facilitating robust cross-domain pre-training. The superior effectiveness of our proposed UniCL is demonstrated by extensive experiments on two benchmarks across eleven domains.

REFERENCES

- [1] Abdul Fatir Ansari, Lorenzo Stella, Caner Turkmen, Xiyuan Zhang, Pedro Mercado, Huibin Shen, Oleksandr Shchur, Syama Sundar Rangapuram, Sebastian Pineda Arango, Shubham Kapoor, et al. 2024. Chronos: Learning the Language of Time Series. *arXiv preprint arXiv:2403.07815* (2024).
- [2] Anthony Bagnall, Hoang Anh Dau, Jason Lines, Michael Flynn, James Large, Aaron Bostrom, Paul Southam, and Eamonn Keogh. 2018. The UEA multivariate time series classification archive, 2018. *arXiv preprint arXiv:1811.00075* (2018).
- [3] Yuxuan Bian, Xuan Ju, Jiangtong Li, Zhijian Xu, Dawei Cheng, and Qiang Xu. 2024. Multi-Patch Prediction: Adapting LLMs for Time Series Representation Learning. *arXiv preprint arXiv:2402.04852* (2024).
- [4] Ching Chang, Wen-Chih Peng, and Tien-Fu Chen. 2023. Llm4ts: Two-stage fine-tuning for time-series forecasting with pre-trained llms. *arXiv preprint arXiv:2308.08469* (2023).
- [5] Tianqi Chen and Carlos Guestrin. 2016. Xgboost: A scalable tree boosting system. In *Proceedings of the 22nd acm sigkdd international conference on knowledge discovery and data mining*. 785–794.
- [6] Ting Chen, Simon Kornblith, Mohammad Norouzi, and Geoffrey Hinton. 2020. A simple framework for contrastive learning of visual representations. In *International conference on machine learning*. PMLR, 1597–1607.
- [7] Yakun Chen, Xianzhi Wang, and Guandong Xu. 2023. Gatgpt: A pre-trained large language model with graph attention network for spatiotemporal imputation. *arXiv preprint arXiv:2311.14332* (2023).
- [8] Mingyue Cheng, Qi Liu, Zhiding Liu, Hao Zhang, Ruijiao Zhang, and Enhong Chen. 2023. Timemae: Self-supervised representations of time series with decoupled masked autoencoders. *arXiv preprint arXiv:2303.00320* (2023).
- [9] Hoang Anh Dau, Anthony Bagnall, Kaveh Kamgar, Chin-Chia Michael Yeh, Yan Zhu, Shaghayegh Gharghabi, Chotirat Ann Ratanamahatana, and Eamonn Keogh. 2019. The UCR time series archive. *IEEE/CAA Journal of Automatica Sinica* 6, 6 (2019), 1293–1305.
- [10] Angus Dempster, François Petitjean, and Geoffrey I Webb. 2020. ROCKET: exceptionally fast and accurate time series classification using random convolutional kernels. *Data Mining and Knowledge Discovery* 34, 5 (2020), 1454–1495.
- [11] Jacob Devlin, Ming-Wei Chang, Kenton Lee, and Kristina Toutanova. 2018. Bert: Pre-training of deep bidirectional transformers for language understanding. *arXiv preprint arXiv:1810.04805* (2018).
- [12] Jiaxiang Dong, Haixu Wu, Haoran Zhang, Li Zhang, Jianmin Wang, and Ming-sheng Long. 2024. Simmtm: A simple pre-training framework for masked time-series modeling. *Advances in Neural Information Processing Systems* 36 (2024).
- [13] Emadelddeen Eldele, Mohamed Ragab, Zhenghua Chen, Min Wu, Chee Keong Kwok, Xiaoli Li, and Cuntai Guan. 2021. Time-Series Representation Learning via Temporal and Contextual Contrasting. In *Proceedings of the Thirtieth International Joint Conference on Artificial Intelligence, IJCAI-21*. 2352–2359.
- [14] Haoyi Fan, Fengbin Zhang, and Yue Gao. 2020. Self-supervised time series representation learning by inter-intra relational reasoning. *arXiv preprint arXiv:2011.13548* (2020).
- [15] Jean-Yves Franceschi, Aymeric Dieuleveut, and Martin Jaggi. 2019. Unsupervised scalable representation learning for multivariate time series. *Advances in neural information processing systems* 32 (2019).
- [16] Shanghua Gao, Teddy Koker, Owen Queen, Thomas Hartvigsen, Theodoros Tsiligkaridis, and Marinka Zitnik. 2024. UniTS: Building a Unified Time Series Model. *arXiv preprint arXiv:2403.00131* (2024).
- [17] Rakshitha Wahsadini Godahewa, Christoph Bergmeir, Geoffrey I. Webb, Rob Hyndman, and Pablo Montero-Manso. 2021. Monash Time Series Forecasting Archive. In *Thirty-fifth Conference on Neural Information Processing Systems Datasets and Benchmarks Track (Round 2)*.
- [18] Ian J Goodfellow, Mehdi Mirza, Da Xiao, Aaron Courville, and Yoshua Bengio. 2013. An empirical investigation of catastrophic forgetting in gradient-based neural networks. *arXiv preprint arXiv:1312.6211* (2013).
- [19] Edward J Hu, Yelong Shen, Phillip Wallis, Zeyuan Allen-Zhu, Yuanzhi Li, Shean Wang, Lu Wang, and Weizhu Chen. 2021. Lora: Low-rank adaptation of large language models. *arXiv preprint arXiv:2106.09685* (2021).
- [20] Zhaoyang Huang, Xiaoyu Shi, Chao Zhang, Qiang Wang, Ka Chun Cheung, Hongwei Qin, Jifeng Dai, and Hongsheng Li. 2022. Flowformer: A transformer architecture for optical flow. In *European conference on computer vision*. Springer, 668–685.
- [21] Hassan Ismail Fawaz, Germain Forestier, Jonathan Weber, Lhassane Idoumghar, and Pierre-Alain Muller. 2019. Deep learning for time series classification: a review. *Data mining and knowledge discovery* 33, 4 (2019), 917–963.
- [22] Ming Jin, Shiyu Wang, Lintao Ma, Zhixuan Chu, James Y Zhang, Xiaoming Shi, Pin-Yu Chen, Yuxuan Liang, Yuan-Fang Li, Shirui Pan, and Qingsong Wen. 2024. Time-LLM: Time series forecasting by reprogramming large language models. In *International Conference on Learning Representations (ICLR)*.
- [23] Ming Jin, Qingsong Wen, Yuxuan Liang, Chaoli Zhang, Siqiao Xue, Xue Wang, James Zhang, Yi Wang, Haifeng Chen, Xiaoli Li, et al. 2023. Large models for time series and spatio-temporal data: A survey and outlook. *arXiv preprint arXiv:2310.10196* (2023).
- [24] Bulat Khaertdinov, Esam Ghaleb, and Stylianos Asteriadis. 2021. Contrastive self-supervised learning for sensor-based human activity recognition. In *2021 IEEE International Joint Conference on Biometrics (IJCB)*. IEEE, 1–8.
- [25] Dani Kiyasseh, Tingting Zhu, and David A Clifton. 2021. Clocs: Contrastive learning of cardiac signals across space, time, and patients. In *International Conference on Machine Learning*. PMLR, 5606–5615.
- [26] Bee Hock David Koh, Chin Leng Peter Lim, Hasnae Rahimi, Wai Lok Woo, and Bin Gao. 2021. Deep temporal convolution network for time series classification. *Sensors* 21, 2 (2021), 603.
- [27] Guokun Lai, Wei-Cheng Chang, Yiming Yang, and Hanxiao Liu. 2018. Modeling long-and short-term temporal patterns with deep neural networks. In *The 41st international ACM SIGIR conference on research & development in information retrieval*. 95–104.
- [28] Zhe Li, Zhongwen Rao, Lujia Pan, Pengyun Wang, and Zenglin Xu. 2023. Ti-mae: Self-supervised masked time series autoencoders. *arXiv preprint arXiv:2301.08871* (2023).
- [29] Zhiyu Liang, Jianfeng Zhang, Chen Liang, Hongzhi Wang, Zheng Liang, and Lujia Pan. 2023. Contrastive shapelet learning for unsupervised multivariate time series representation learning. *arXiv preprint arXiv:2305.18888* (2023).
- [30] Bryan Lim and Stefan Zohren. 2021. Time-series forecasting with deep learning: a survey. *Philosophical Transactions of the Royal Society A* 379, 2194 (2021), 20200209.
- [31] Chen Liu, Shibo He, Qihang Zhou, Shizhong Li, and Wenchao Meng. 2024. Large Language Model Guided Knowledge Distillation for Time Series Anomaly Detection. *arXiv preprint arXiv:2401.15123* (2024).
- [32] Haoxin Liu, Zhiyuan Zhao, Jindong Wang, Harshavardhan Kamarthi, and B Aditya Prakash. 2024. LSTPrompt: Large Language Models as Zero-Shot Time Series Forecasters by Long-Short-Term Prompting. *arXiv preprint arXiv:2402.16132* (2024).
- [33] Jiexi Liu and Songcan Chen. 2024. Timesurl: Self-supervised contrastive learning for universal time series representation learning. In *Proceedings of the AAAI Conference on Artificial Intelligence*, Vol. 38. 13918–13926.
- [34] Peiyuan Liu, Hang Guo, Tao Dai, Naiqi Li, Jigang Bao, Xudong Ren, Yong Jiang, and Shu-Tao Xia. 2024. Taming Pre-trained LLMs for Generalised Time Series Forecasting via Cross-modal Knowledge Distillation. *arXiv preprint arXiv:2403.07300* (2024).
- [35] Shizhan Liu, Hang Yu, Cong Liao, Jianguo Li, Weiyao Lin, Alex X Liu, and Schahram Dustdar. 2021. Pyraformer: Low-complexity pyramidal attention for long-range time series modeling and forecasting. In *International conference on learning representations*.
- [36] Xu Liu, Junfeng Hu, Yuan Li, Shizhe Diao, Yuxuan Liang, Bryan Hooi, and Roger Zimmermann. 2023. Unimate: A language-empowered unified model for cross-domain time series forecasting. *arXiv preprint arXiv:2310.09751* (2023).
- [37] Yong Liu, Guo Qin, Xiangdong Huang, Jianmin Wang, and Mingsheng Long. 2024. AutoTimes: Autoregressive Time Series Forecasters via Large Language Models. *arXiv preprint arXiv:2402.02370* (2024).
- [38] Yong Liu, Haixu Wu, Jianmin Wang, and Mingsheng Long. 2022. Non-stationary transformers: Exploring the stationarity in time series forecasting. *Advances in Neural Information Processing Systems* 35 (2022), 9881–9893.
- [39] Dongsheng Luo, Wei Cheng, Yingheng Wang, Dongkuan Xu, Jingchao Ni, Wen-chao Yu, Xuchao Zhang, Yanchi Liu, Yuncong Chen, Haifeng Chen, et al. 2023. Time series contrastive learning with information-aware augmentations. In *Proceedings of the AAAI Conference on Artificial Intelligence*, Vol. 37. 4534–4542.
- [40] Qianli Ma, Zhen Liu, Zhenjing Zheng, Ziyang Huang, Siying Zhu, Zhongzhong Yu, and James T Kwok. 2023. A survey on time-series pre-trained models. *arXiv preprint arXiv:2305.10716* (2023).
- [41] Qianwen Meng, Hangwei Qian, Yong Liu, Lizhen Cui, Yonghui Xu, and Zhiqi Shen. 2023. MHCCCL: masked hierarchical cluster-wise contrastive learning for multivariate time series. In *Proceedings of the AAAI Conference on Artificial Intelligence*, Vol. 37. 9153–9161.
- [42] Shikai Qiu, Nate Gruver, Marc Finzi, and Andrew Gordon Wilson. 2023. Large Language Models Are Zero Shot Time Series Forecasters. In *Advances in Neural Information Processing Systems*.
- [43] Yuqi Nie, Nam H. Nguyen, Phanwadee Sinthong, and Jayant Kananam. 2023. A Time Series is Worth 64 Words: Long-term Forecasting with Transformers. In *International Conference on Learning Representations*.
- [44] Saeed Amizadeh Nikolay Laptev, Y. B. 2015. A Benchmark Dataset for Time Series Anomaly Detection. <https://yahooresearch.tumblr.com/post/114590420346/a-benchmark-dataset-for-time-series-anomaly>
- [45] OpenAI. 2022. OpenAI: Introducing ChatGPT. <https://openai.com/blog/chatgpt>
- [46] Yilmazcan Ozyurt, Stefan Feuerriegel, and Ce Zhang. 2023. Contrastive Learning for Unsupervised Domain Adaptation of Time Series. *ICLR* (2023).
- [47] Johannes Pöppelbaum, Gavneet Singh Chadha, and Andreas Schwung. 2022. Contrastive learning based self-supervised time-series analysis. *Applied Soft Computing* 117 (2022), 108397.
- [48] Xiangfei Qiu, Jilin Hu, Lekui Zhou, Xingjian Wu, Junyang Du, Buang Zhang, Chenjuan Guo, Aoying Zhou, Christian S Jensen, Zhenli Sheng, and Bin Yang.

2024. TFB: Towards Comprehensive and Fair Benchmarking of Time Series Forecasting Methods. *arXiv preprint arXiv:2403.20150* (2024).
- [49] Alec Radford, Jong Wook Kim, Chris Hallacy, Aditya Ramesh, Gabriel Goh, Sandhini Agarwal, Girish Sastry, Amanda Askell, Pamela Mishkin, Jack Clark, et al. 2021. Learning transferable visual models from natural language supervision. In *International conference on machine learning*. PMLR, 8748–8763.
- [50] Alec Radford, Jeffrey Wu, Rewon Child, David Luan, Dario Amodei, Ilya Sutskever, et al. 2019. Language models are unsupervised multitask learners. *OpenAI blog* 1, 8 (2019), 9.
- [51] Colin Raffel, Noam Shazeer, Adam Roberts, Katherine Lee, Sharan Narang, Michael Matena, Yanqi Zhou, Wei Li, and Peter J. Liu. 2020. Exploring the Limits of Transfer Learning with a Unified Text-to-Text Transformer. *Journal of Machine Learning Research* 21, 140 (2020), 1–67. <http://jmlr.org/papers/v21/20-074.html>
- [52] Aniruddh Raghu, Payal Chandak, Ridwan Alam, John Gutttag, and Collin Stultz. 2023. Sequential multi-dimensional self-supervised learning for clinical time series. In *International Conference on Machine Learning*. PMLR, 28531–28548.
- [53] Kashif Rasul, Arjun Ashok, Andrew Robert Williams, Arian Khorasani, George Adamopoulos, Rishika Bhagwatkar, Marin Biloš, Hena Ghonia, Nadhir Vincent Hassen, Anderson Schneider, et al. 2023. Lag-llama: Towards foundation models for time series forecasting. *arXiv preprint arXiv:2310.08278* (2023).
- [54] Hansheng Ren, Bixiong Xu, Yujing Wang, Chao Yi, Congrui Huang, Xiaoyu Kou, Tony Xing, Mao Yang, Jie Tong, and Qi Zhang. 2019. Time-Series Anomaly Detection Service at Microsoft. In *Proceedings of the 25th ACM SIGKDD International Conference on Knowledge Discovery & Data Mining (KDD '19)*. Association for Computing Machinery, 3009–3017. <https://doi.org/10.1145/3292500.3330680>
- [55] Hojjat Salehinejad, Sharan Sankar, Joseph Barfett, Errol Colak, and Shahrokh Valaei. 2017. Recent advances in recurrent neural networks. *arXiv preprint arXiv:1801.01078* (2017).
- [56] Nikunj Saunshi, Orestis Plevrakis, Sanjeev Arora, Mikhail Khodak, and Hrishikesh Khandeparkar. 2019. A theoretical analysis of contrastive unsupervised representation learning. In *International Conference on Machine Learning*. PMLR, 5628–5637.
- [57] Omer Berat Sezer, Mehmet Ugur Gudelek, and Ahmet Murat Ozbayoglu. 2020. Financial time series forecasting with deep learning: A systematic literature review: 2005–2019. *Applied soft computing* 90 (2020), 106181.
- [58] Chenxi Sun, Yaliang Li, Hongyan Li, and Shenda Hong. 2023. TEST: Text prototype aligned embedding to activate LLM’s ability for time series. *arXiv preprint arXiv:2308.08241* (2023).
- [59] Xue Wang, Liang Sun, Rong Jin, Tian Zhou, Peisong Niu. 2023. One Fits All: Power General Time Series Analysis by Pretrained LM. In *NeurIPS*.
- [60] Sana Tonekaboni, Danny Eytan, and Anna Goldenberg. 2021. Unsupervised Representation Learning for Time Series with Temporal Neighborhood Coding. In *International Conference on Learning Representations*. <https://openreview.net/forum?id=8qDweJCUCN>
- [61] Hugo Touvron, Thibaut Lavril, Gautier Izacard, Xavier Martinet, Marie-Anne Lachaux, Timothée Lacroix, Baptiste Rozière, Naman Goyal, Eric Hambro, Faisal Azhar, Aurelien Rodriguez, Armand Joulin, Edouard Grave, and Guillaume Lample. 2023. LLaMA: Open and Efficient Foundation Language Models. *ArXiv abs/2302.13971* (2023).
- [62] Patara Tirat, Yooju Shin, Junhyeok Kang, Youngeun Nam, Jihye Na, Minyoung Bae, Joehun Kim, Byunghyun Kim, and Jae-Gil Lee. 2024. Universal Time-Series Representation Learning: A Survey. *arXiv preprint arXiv:2401.03717* (2024).
- [63] Yihe Wang, Yu Han, Haishuai Wang, and Xiang Zhang. 2024. Contrast everything: A hierarchical contrastive framework for medical time-series. *Advances in Neural Information Processing Systems* 36 (2024).
- [64] Qingsong Wen, Linxiao Yang, Tian Zhou, and Liang Sun. 2022. Robust time series analysis and applications: An industrial perspective. In *Proceedings of the 28th ACM SIGKDD Conference on Knowledge Discovery and Data Mining*. 4836–4837.
- [65] Qingsong Wen, Tian Zhou, Chaoli Zhang, Weiqi Chen, Ziqing Ma, Junchi Yan, and Liang Sun. 2022. Transformers in time series: A survey. *arXiv preprint arXiv:2202.07125* (2022).
- [66] Gerald Woo, Chenghao Liu, Doyen Sahoo, Akshat Kumar, and Steven Hoi. 2022. CoST: Contrastive Learning of Disentangled Seasonal-Trend Representations for Time Series Forecasting. In *International Conference on Learning Representations*. <https://openreview.net/forum?id=PilZY3omXV2>
- [67] Gerald Woo, Chenghao Liu, Doyen Sahoo, Akshat Kumar, and Steven C. H. Hoi. 2022. ETSformer: Exponential Smoothing Transformers for Time-series Forecasting. (2022). <https://arxiv.org/abs/2202.01381>
- [68] Haixu Wu, Tengge Hu, Yong Liu, Hang Zhou, Jianmin Wang, and Mingsheng Long. 2023. TimesNet: Temporal 2D-Variation Modeling for General Time Series Analysis. In *International Conference on Learning Representations*.
- [69] Haixu Wu, Jiehui Xu, Jianmin Wang, and Mingsheng Long. 2021. Autoformer: Decomposition transformers with auto-correlation for long-term series forecasting. *Advances in neural information processing systems* 34 (2021), 22419–22430.
- [70] Hao Xue and Flora D Salim. 2023. Promptcast: A new prompt-based learning paradigm for time series forecasting. *IEEE Transactions on Knowledge and Data Engineering* (2023).
- [71] Chin-Chia Michael Yeh, Xin Dai, Huiyuan Chen, Yan Zheng, Yujie Fan, Audrey Der, Vivian Lai, Zhongfang Zhuang, Junpeng Wang, Liang Wang, et al. 2023. Toward a foundation model for time series data. In *Proceedings of the 32nd ACM International Conference on Information and Knowledge Management*. 4400–4404.
- [72] Zhihan Yue, Yujing Wang, Juanyong Duan, Tianmeng Yang, Congrui Huang, Yunhai Tong, and Bixiong Xu. 2022. Ts2vec: Towards universal representation of time series. In *Proceedings of the AAAI Conference on Artificial Intelligence*. Vol. 36. 8980–8987.
- [73] Ailing Zeng, Muxi Chen, Lei Zhang, and Qiang Xu. 2023. Are transformers effective for time series forecasting?. In *Proceedings of the AAAI conference on artificial intelligence*. Vol. 37. 11121–11128.
- [74] George Zerveas, Srideepika Jayaraman, Dhaval Patel, Anuradha Bhamidipaty, and Carsten Eickhoff. 2021. A transformer-based framework for multivariate time series representation learning. In *Proceedings of the 27th ACM SIGKDD conference on knowledge discovery & data mining*. 2114–2124.
- [75] Kexin Zhang, Qingsong Wen, Chaoli Zhang, Rongyao Cai, Ming Jin, Yong Liu, James Zhang, Yuxuan Liang, Guansong Pang, Dongjin Song, and Shirui Pan. 2023. Self-Supervised Learning for Time Series Analysis: Taxonomy, Progress, and Prospects. *arXiv preprint arXiv:2306.10125* (2023).
- [76] Kexin Zhang, Qingsong Wen, Chaoli Zhang, Rongyao Cai, Ming Jin, Yong Liu, James Y Zhang, Yuxuan Liang, Guansong Pang, Dongjin Song, et al. 2024. Self-supervised learning for time series analysis: Taxonomy, progress, and prospects. *IEEE Transactions on Pattern Analysis and Machine Intelligence* (2024).
- [77] Tianping Zhang, Yizhuo Zhang, Wei Cao, Jiang Bian, Xiaohan Yi, Shun Zheng, and Jian Li. 2022. Less is more: Fast multivariate time series forecasting with light sampling-oriented mlp structures. *arXiv preprint arXiv:2207.01186* (2022).
- [78] Xiang Zhang, Ziyuan Zhao, Theodoros Tsiligkaridis, and Marinka Zitnik. 2022. Self-supervised contrastive pre-training for time series via time-frequency consistency. *Advances in Neural Information Processing Systems* 35 (2022), 3988–4003.
- [79] Yifei Zhang, Hao Zhu, Zixing Song, Piotr Koniusz, and Irwin King. 2022. COSTA: covariance-preserving feature augmentation for graph contrastive learning. In *Proceedings of the 28th ACM SIGKDD Conference on Knowledge Discovery and Data Mining*. 2524–2534.
- [80] Bendong Zhao, Huanzhang Lu, Shangfeng Chen, Junliang Liu, and Dongya Wu. 2017. Convolutional neural networks for time series classification. *Journal of Systems Engineering and Electronics* 28, 1 (2017), 162–169.
- [81] Xiaochen Zheng, Xing-Yu Chen, Manuel Schurch, Amina Mollaysa, Ahmed Al-lam, and M. Krauthammer. 2023. SimTS: Rethinking Contrastive Representation Learning for Time Series Forecasting. *ArXiv abs/2303.18205* (2023).
- [82] Haoyi Zhou, Shanghang Zhang, Jieqi Peng, Shuai Zhang, Jianxin Li, Hui Xiong, and Wancai Zhang. 2021. Informer: Beyond efficient transformer for long sequence time-series forecasting. In *Proceedings of the AAAI conference on artificial intelligence*. Vol. 35. 11106–11115.
- [83] Tian Zhou, Ziqing Ma, Qingsong Wen, Xue Wang, Liang Sun, and Rong Jin. 2022. Fedformer: Frequency enhanced decomposed transformer for long-term series forecasting. In *International conference on machine learning*. PMLR, 27268–27286.